ADVANCED ENERGY MATERIALS
www.advenergymat.de

Insights into Li-Rich Mn-Based Cathode Materials with High Capacity: from Dimension to Lattice to Atom

Shao-Lun Cui, Ming-Yue Gao, Guo-Ran Li, and Xue-Ping Gao*

Li-rich Mn-based layered oxides are regarded as the most promising cathode materials for advanced lithium-ion batteries with energy density as high as 400 Wh kg^{-1}. However, decline of capacity and discharge potential derived from phase transformation during cycling is still an obstacle for practical utilization of Li-rich cathode materials. Undoubtedly, an in-depth understanding origin and evolution of the phase transformation from bottom to top is crucial to solve the problem finally. Herein, the recent representative progress on Li-rich cathode materials from top to bottom is summarized: starting from relationship between dimensions and performance, to evolution of phase transformation, finally to participation of anions during charge–discharge cycling. It systematically shows what happens in the different microscopic levels and how these phenomena relate to cycling of Li-rich cathode materials with the help of emerging state-of-the-art characterization techniques. On the basis of this progress, it is proposed that rational structural design can fully play its role to build high-performance energy storage materials and enhance structural stability.

1. Introduction

The prosperity of layered Li-rich Mn-based cathode materials, represented as $x\mathrm{Li_2MnO_3}\cdot(1\text{–}x)\mathrm{LiMO_2}$ (M = transition metal), has injected new vitality into the next generation of high-energy lithium-ion batteries.[1–3] Compared with traditional lithium ion cathode materials, such as layered $\mathrm{LiCoO_2}$, olivine $\mathrm{LiFePO_4}$, and Ni-rich cathode materials, Li-rich Mn-based cathode materials can deliver high discharge capacities of more than 250 mAh g^{-1} with low cost and low toxicity.[4,5] Li-rich Mn-based cathode materials was first proposed by Thackeray and co-workers in 1991, which gained extensive attention in the past decade.[1] However, its inherent shortcomings, including low initial Coulombic efficiency, poor cycling performance, severe voltage decay, and wide voltage range, hinder its practical application in electric vehicles and portable electronic devices. In addition, the harsh working environment, especially the low-temperature condition, will cause the sluggish kinetics of electrode reaction by suppressing the Mn^{4+}/Mn^{3+} reduction reaction.[3c] Although a series of effective coating, doping and structural design strategies previously reported have been put into practice and significantly improved the electrochemical performance and structural stability from the macro perspective, plenty of the underlying and fundamental reaction mechanisms have not yet been elucidated clearly.[6–8] From a more microscopic dimension, root of the decline in electrochemical performance include escape of oxygen atoms, redox of cations and anions, and phase transformation, in which such microscopic characterizations require cutting-edge technologies. Recently, tremendous efforts have been devoted to investigating complex reaction mechanisms behind the structure with the help of state-of-the-art characterization techniques.[8]

In general, the superior electrochemical behavior of Li-rich Mn-based cathode materials is not only derived from the contribution of transition metal cations, but also closely related to the anionic redox activity, especially reflected in the unique first charge process.[9] The initial charge process usually consists of two regions: sloping region and plateau region. The first stage occurs below 4.4 V, and lithium ions are extracted from the lithium layer along with the oxidation of transition metal ions to high valence state.[10,11] While the second stage presents a long plateau that appears above 4.4 V and stands for the activation of $\mathrm{Li_2MnO_3}$ phase. During the plateau region, lithium ions are continuously extracted and interact with oxygen in the form of Li–O–Li configuration as charge compensation.[12] Whereas, the specific role and mechanism of anionic redox activity in electrochemical reactions are still in dispute. This is because oxygen can participate in both reversible and irreversible redox reactions. What kind of intermediate form does oxygen take part in the reversible process? Where does the irreversible oxygen loss originate from, bulk lattice or electrolyte oxidation? How do these two parts contribute to capacities independently and influence mutually? These issues seriously challenge further development and need to be clarified in detail. In addition, the original structure is prone to transition metal migration and phase transformation due to anionic redox activities.[13,14] It is worth noting that not only the intrinsic structure of Li-rich Mn-based cathode materials is very complicated, but also its evolution mechanism of phase transformation during cycling is even more controversial. Furthermore, the lack of powerful characterization tools

---

S.-L. Cui, M.-Y. Gao, Prof. G.-R. Li, Prof. X.-P. Gao
Institute of New Energy Material Chemistry
School of Materials Science and Engineering
Renewable Energy Conversion and Storage Center
Nankai University
Tianjin 300350, China
E-mail: guoranli@nankai.edu.cn

The ORCID identification number(s) for the author(s) of this article can be found under https://doi.org/10.1002/aenm.202003885.

DOI: 10.1002/aenm.202003885

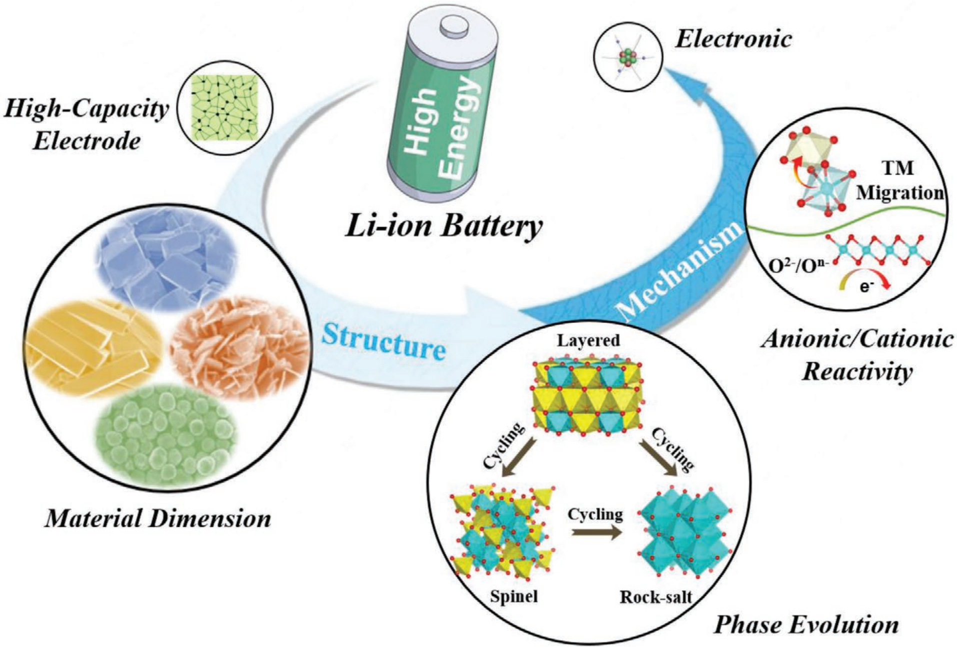

Scheme 1. Schematic diagram of the mechanism of Li-rich Mn-based cathode materials from a macro to micro perspective.

to observe from a microscopic perspective inevitably limited the overall understanding of its structural degradation in the past. It is not until recently that researchers focus on the reaction mechanisms behind anionic redox and phase evolution at molecular and atomic levels, which are mainly responsible for capacity fading and voltage decay. These advancements have greatly improved our knowledge of Li-rich Mn-based cathode materials and provided guidance on how to achieve precise multidimensional structure design. As illustrated in **Scheme 1**, we summarize a comprehensive review aimed at introducing the latest progress in multidimensional structure, phase transformation, and anionic redox activity from a macro to a micro perspective. Based on revealing the reaction mechanism, future perspectives are also presented for the inspiration of higher-performance energy storage materials.

2. Relationships between Dimensions and Performance

Nanostructured electrode materials for lithium-ion batteries are usually beneficial for improving electrochemical performance, because the small size can not only shorten lithium-ion diffusion path and provide a large specific surface area for electrochemical reactions, but also promote the thermodynamic and kinetic factors of the interface electrochemical reaction. So far, the structures of Li-rich Mn-based cathode materials, including multidimensional structures, core–shell structure, full concentration-gradient structures, and composite structure have made significant progress in the past decades.

Multidimensional structure of Li-rich Mn-based cathode materials usually refers to the synthesis of energy storage materials with different dimensions and morphologies via diverse methods. Moreover, it tends to be functional structures of specific properties with micro or even nanometer-scale feature sizes through rational design. On the one hand, it can promote the dynamics of the electrode process, especially to ensure the smooth progress of the Li^+ diffusion at the interface and bulk phase. On the other hand, the regular morphology and size can further increase the energy density and tap density of the Li-rich Mn-based cathode material, thereby improving the utilization of active materials.

The synthesis and preparation of 1D micro–nano-structured cathode materials with controllable morphology and composition is extremely attractive and challenging for the research of Li-rich Mn-based cathode materials. 1D micro–nano structure refers to a micro–nano structure with 1D characteristics including nanorods, nanowires, and nanotubes. The 1D micro–nano-structured cathode material can greatly shorten the diffusion path of electrons and lithium ions, ensure a more sufficient contact area between the cathode material and the electrolyte, and suppress the strain during the insertion and extraction of lithium ions. In addition, the 1D Li-rich Mn-based cathode material can inhibit the irreversible phase transformation during cycling to a certain extent and accelerate the dynamic process, thereby improving its intrinsic stability. So far, 1D micro–nano-structured cathode materials are difficult to synthesize due to poor composition and shape controllability, uneven size distribution, and difficulty in large-scale preparation. For this reason, researchers have spent a lot of time and efforts on the synthesis of 1D micro–nano-structured cathode materials. For example, Lee et al.[15a] applied $Co_{0.4}Mn_{0.6}O_2$ nanowires and lithium nitrate as precursors at 200 °C to directly synthesize a high-capacity lithium-ion storage material of $Li_{0.88}[Li_{0.18}Co_{0.33}Mn_{0.49}]O_2$ nanowires by hydrothermal method. The obtained nanowires exhibited a reversible capacity of 230 mAh g^{-1} between 2.0 and 4.8 V, even at a high rate of 3600 mA g^{-1}. It was also reported that the $Li_{1.23}Mn_{0.538}Ni0_{.117}Co_{0.114}O_2$ cathode material composed of nanofibers was synthesized through the electrospinning process.[15b] A high reversible capacity of 275 mAh g^{-1} was obtained in the fibrous cathode, which also presented superior high-rate capability. In addition, Liu et al.[15c] reported the synthesis and electrochemical application of 1D heterostructured spinel/layered $Li_{1.15}Ni_{0.20}Mn_{0.87}O_2$ nanofibers. The synergistic effect of the 1D nanostructure and the spinel/layered heterostructure improved the charge transfer, Li^+ diffusion rate and structural stability, thereby increasing the initial Coulombic efficiency (100%), rate performance (150 mAh g^{-1} at 5C rate) and cycle performance (258 mAh g^{-1} after 70 cycles). Absolutely, how to design a general strategy for the large-scale preparation of 1D micro–nano-structured Li-rich Mn-based cathode materials with controllable composition and narrow size distribution has received increasing attention in recent years. In respect to thermal stability, Ma et al.[15d] proposed a simple, versatile and mild approach to construct 1D micro–nano-structured Li-rich Mn-based cathode materials with high energy and power density through reasonable selection of precipitating solvents. It was found that lowering the dielectric constant and changing the solute–solvent interaction could lower the nucleation barrier. They successfully overcame the difficulties of uneven size distribution and uncontrollable aspect ratio of 1D cathode materials via an optimized ethanol–water cosolvent, and achieved the goal of large-scale preparation of 1D cathode materials under mild conditions. As shown in **Figure 1**a, homogeneous metal oxalate hydrate ($MC_2O_4\cdot xH_2O$; M = Mn, Ni, Co, and Li) microbars were prepared by precipitation method at room temperature in an ethanol–water cosolvent with optimized ratio. The following postannealing treatment transformed the precursor into the targeted $0.5Li_2MnO_3\cdot 0.5LiNi_{1/3}Co_{1/3}Mn_{1/3}O_2$ cathode material in a topological manner, and the overall morphology was retained. The FESEM and TEM images in Figure 1b–e showed that the obtained sample consisted of uniform microbars with lengths of 6.4 ± 0.4 µm and widths of 1.2 ± 0.2 µm, which was consistent with the bar-like architecture of the $MC_2O_4\cdot xH_2O$ precursor. By controlling the volume ratio of ethanol to water during the synthesis process, the aspect ratio of the microbar precursor could be adjusted. Furthermore, the HRTEM image in Figure 1f and SAED pattern in Figure 1g demonstrated that the as-prepared sample could be well indexed to the layered $LiMO_2$ ($R\bar{3}m$ space group) and Li_2MnO_3 ($C2/m$ space group) phases. It is noteworthy that the secondary particles of the microbar inevitably appear polycrystalline due to the heat treatment process. To be precise, it belongs to a 1D morphology. Based on adjusting the kinetics of crystal nucleation and growth with the ethanol–water ratio of the precipitation solvent, the coordinated solvent tuning strategy was verified to be beneficial for the precise design of 1D micro–nano structure. The harsh synthesis conditions of 1D micro–nano-structured cathode materials limit its further development. How to synthesize cathode materials with a controllable size to meet the needs of industrial production has become an urgent problem to be solved. In addition, it is difficult for traditional nanowires and nanotubes to achieve a high-volume energy density. Correspondingly, choosing a suitable cosolvent can effectively reduce its nucleation barrier and realize large-scale production under mild conditions. By adjusting its aspect ratio and directional assembly of 1D nanoparticles into a structure with higher tap density, the volume energy density can be appropriately increased.

The most prominent feature of the 2D micro–nano-structured cathode material is that it can expose more (010) crystal planes that contribute to lithium-ion transport. Additionally, the structure of the cathode material, especially the surface structure, is a key factor in determining the Li^+ deintercalation/intercalation rate. The ratio of electrochemically active surface for lithium-ion transport is a key criterion for evaluating the high-rate performance of cathode materials with different nanostructures. The 2D micro–nano-structured cathode material can greatly improve the rate performance by increasing the yield of the (010)-nanoplate material, and enhance the surface electrochemical activity. However, the vast majority of nanoplates are thermodynamic equilibrium products by reacting for a long enough time under hydrothermal conditions. Therefore, nanoplates are always less attractive in terms of rate performance. And the typical representative of this type of structure is the plate-like nanoparticles. Previously, Wei et al.[16a] reported a crystal habit-tuned nanoplate cathode material of $Li_{1.17}Ni_{0.25}Mn_{0.58}O_2$ by adjusting the surface structure. As illustrated in **Figure 2**a, the plane perpendicular to the *c*-axis belonged to the (001) crystal plane, and the planes perpendicular to the (001) crystal plane and parallel to the *a*-axis or the *b*-axis belonged to the (010) and (100) crystal planes, respectively. If a 2D nanoplate grew perpendicular to the [010] or [100] direction, its surface would gradually be occupied by (010) crystal planes, and these crystal planes would become active planes for the insertion and extraction of lithium ions. Since the crystal growth rate of the high-energy plane is faster than that of the low-energy plane, the high-energy plane tends to disappear during the growth process, and the surface of the grown crystal will be dominated by the low-energy plane. The surface energy of (001) plane is lower than that of (010) plane. Therefore, (001) nanoplates tend to be thermodynamic equilibrium products synthesized under hydrothermal conditions for a long enough time in most synthesis routes, which also leads to the unsatisfactory rate performance. Different from the previous synthesis route, the yield of (010) nanoplates is improved by shortening the preheating time of the precursor under hydrothermal conditions in the crystal habit-tuned nanoplate material. The $Li_{1.17}Ni_{0.25}Mn_{0.58}O_2$ material synthesized by the hydrothermal method was composed of 5–9 nm 2D nanoplate primary particles and exposed more (010) crystal planes preferentially. Consequently, it gained a high initial discharge capacity up to 197 mAh g^{-1} at 6 C rate and could still keep a discharge capacity of 186 mAh g^{-1} after 50 cycles. Moreover, Wang et al.[16b] applied the coprecipitation method to synthesize the hydroxide precursor $Ni_{0.25}Mn_{0.75}(OH)_2$. As shown in Figure 2b, the secondary particles with an average size of 1–2 µm were composed of hexagonal shaped nanoplates with a thickness of about 50 nm and lateral dimensions ranging from 200 to 500 nm. And the SAED patterns in Figure 2c–e showed that the precursor was a composite of a dominating $Ni(OH)_2$ phase and a minority Mn_3O_4 phase. The layered ($R\bar{3}m$)-layered ($C2/m$)-spinel (Fd-$3m$) cathode material synthesized by this precursor obtained excellent electrochemical performance. In the hexagonal Li-rich Mn-based layered oxides, lithium ions are more likely to move along the *a*/*b*-axis ((001) planes), perpendicular to

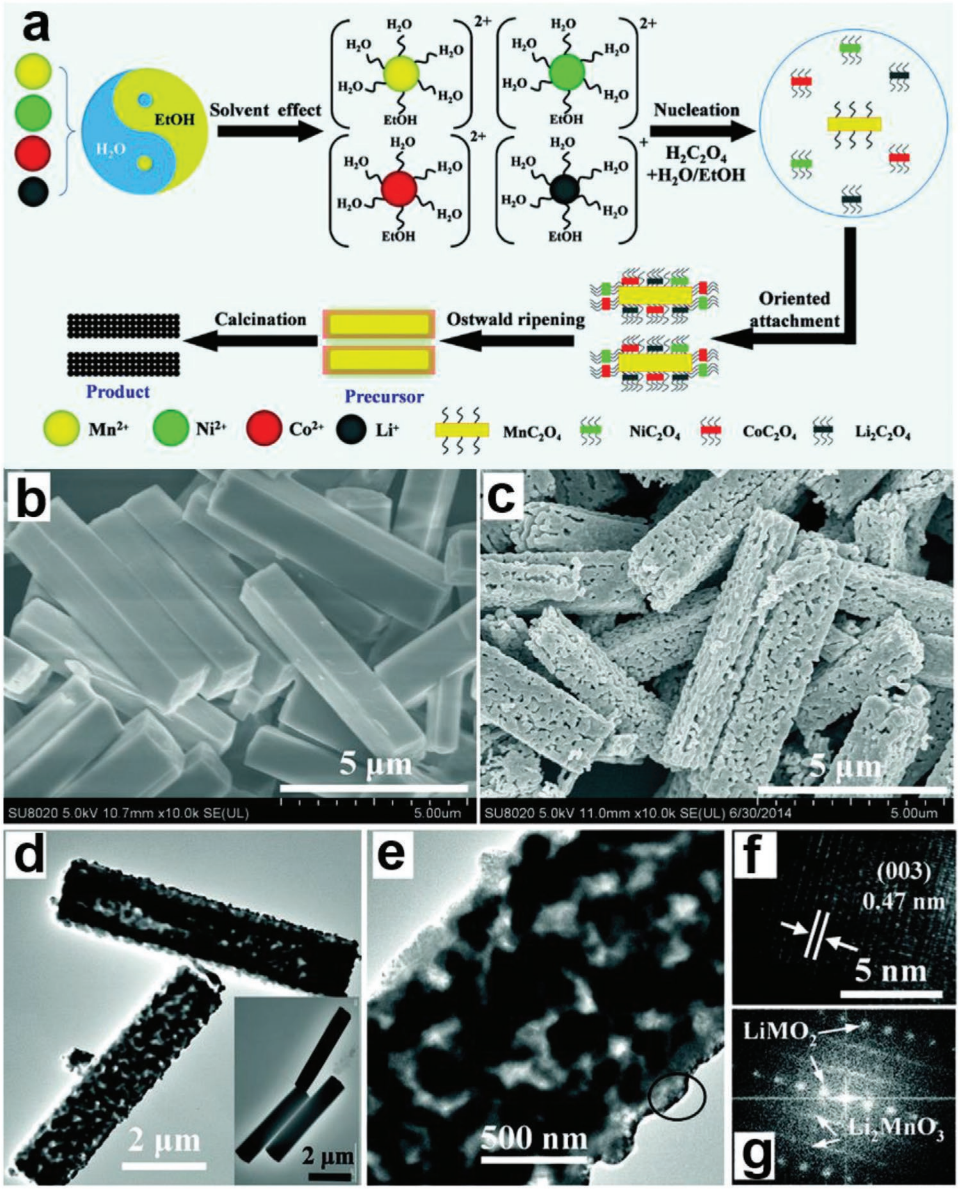

Figure 1. a) Schematic diagram of 1D micro–nano-structured bar-shaped $0.5Li_2MnO_3{\cdot}0.5LiNi_{1/3}Co_{1/3}Mn_{1/3}O_2$ cathode material tuned by ethanol–water cosolvent. b) FESEM image of the metal oxalate hydrate precursor ($MC_2O_4{\cdot}xH_2O$). c) FESEM image of the $0.5Li_2MnO_3{\cdot}0.5LiNi_{1/3}Co_{1/3}Mn_{1/3}O_2$ cathode material. d,e) TEM and HRTEM images of the $0.5Li_2MnO_3{\cdot}0.5LiNi_{1/3}Co_{1/3}Mn_{1/3}O_2$ cathode material. f) HRTEM of the circled region in (e). g) FFT of the HRTEM image in (f). Reproduced with permission.[15d] Copyright 2016, Wiley-VCH.

the *c*-axis. If the surface of the nanoparticle is mostly parallel to the (010), (100), and (110) planes, and perpendicular to the (001) plane, the intercalation/deintercalation rate of lithium ions will be significantly increased. Herein, the 2D nanoplate primary particles are abundant in exposed Li^+ electrochemically active surface, which is conducive to the rapid insertion/extraction of Li^+, while the micrometer-sized secondary particles can ensure the stability of the structure and facilitate the sufficient penetration of the electrolyte at the electrode interface. The synthesis of 2D micro–nano-structured cathode materials often relies on hydrothermal and solvothermal methods, which are accompanied by low yields and high budgets. It has also become one of the biggest obstacles to the commercialization of 2D structures. Besides, how to control the growth process of the 2D structure surface to regulate its electrochemical activity remains a difficulty. Generally, the crystal surface will be occupied by crystal planes with low surface energy. It is proposed that the reaction time and temperature can be adjusted to reduce the surface energy of specific crystal plane growth, so as to improve its rate performance.

A widely reported research area is the design of hierarchical structures, which are micrometer-sized secondary particles composed of nanometer-sized primary particles. The hierarchical structures can generally enhance the rate capability of nanoparticles, reduce electrode/electrolyte side reactions, and achieve higher micrometer-scale particle density. Currently, the most

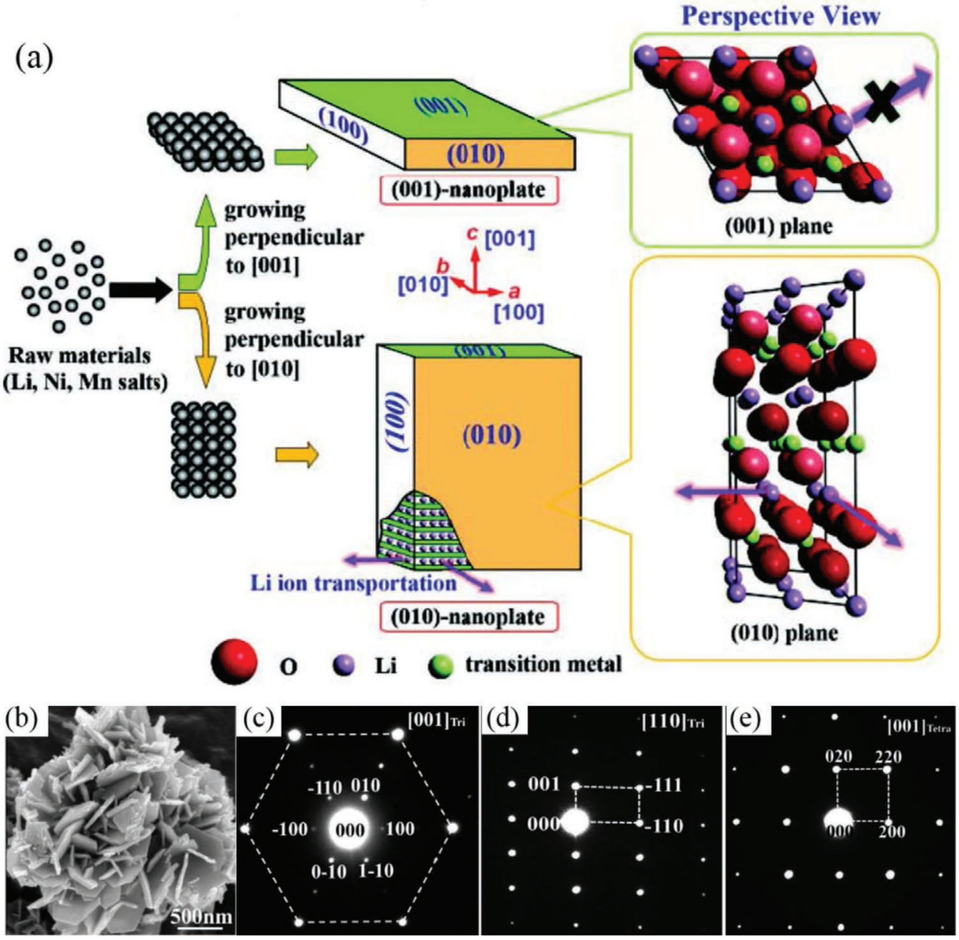

Figure 2. a) Schematic diagram of two nanoplates and their surface structures. Reproduced with permission.[16a] Copyright 2010, Wiley-VCH. b) SEM image of the $Ni_{0.25}Mn_{0.75}(OH)_2$ precursor. c–e) SAED patterns of the $Ni_{0.25}Mn_{0.75}(OH)_2$ precursor along different zone axis. Reproduced with permission.[16b] Copyright 2013, Wiley-VCH.

widely studied and reported hierarchical structure is the 3D spherical cathode material. Microsphere secondary particles are usually formed by agglomeration of nanosized primary particles. The spherical cathode material has excellent fluidity and can be prepared on a large scale under mild synthesis conditions, thus becoming one of the few morphologies that can meet industrial production. It has relatively high economic feasibility and low process limitations. In addition, the microsphere secondary particles have a higher packing density and tap density, which can achieve a higher energy density. However, the microsphere particles also have its own shortcomings. Due to the local strain during the charge and discharge process, microcracks or even breakage is easily generated, which also causes a rapid decline in its capacity. Kim et al.[17a] synthesized $Li[Li_{0.19}Ni_{0.16}Co_{0.08}Mn_{0.57}]O_2$ cathode materials with a specific microstructure and high tap density in flowing air by a coprecipitation method. The spherical secondary particles were composed of sphere-shaped nanoprimary particles and delivered a high gravimetric specific capacity of 263 mAh g^{-1} and a volume specific capacity of 956 mAh cm^{-3}. Compared with the cathode material composed of irregular primary particles, it exhibited a higher packing density. This difference was mainly caused by fewer contact interfaces and vacancies between spherical primary particles. It was reported that the rate performance of $Li_{1.2}Ni_{0.2}Mn_{0.6}O_2$ spherical cathode material at low temperature could be greatly improved by tuning primary particle growth.[17b] To develop high-rate and cycle-stable cathode materials, Zhang et al.[18a] reported a simple and versatile strategy to synthesize a 3D spherical hierarchical $Li_{1.2}Ni_{0.13}Mn_{0.54}Co_{0.13}O_2$ layered cathode material. After mixed with Ni^{2+}, Co^{2+}, and Li^+ salts, the urchin-like α-MnO_2 precursor was converted into the target hierarchical structure during the sintering process. The discharge capacity of the spherical materials was maintained at about 250 mAh g^{-1} with a capacity retention rate of 97% after 50 cycles, and the Coulombic efficiency was close to 100%. In addition, Oh et al.[18b] obtained the superior long-term energy retention and volumetric energy density by preparing 10 μm sized spherical particles composed of sub-micrometer-sized flake-like primary particles, as shown in **Figure 3**a–c. They provided a new activation method, which overcame the limitation of the larger cathode particles in the past, and maximized the volumetric energy density while minimizing the damage to bulk materials caused by surface degradation. In this design, the size and shape of the primary particles effectively reduced the surface area, thereby significantly

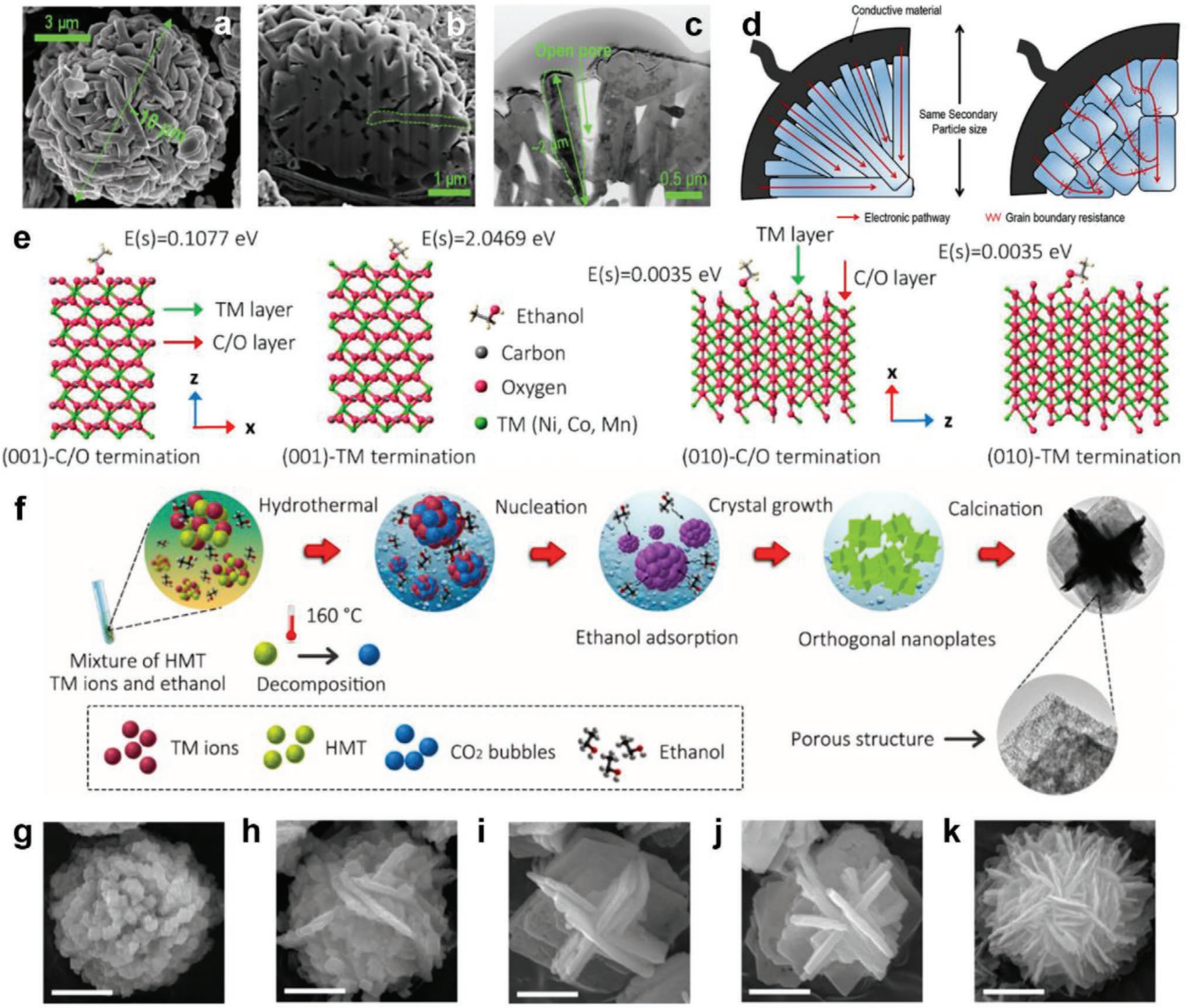

Figure 3. a,b) SEM images of the Li-rich Mn-based spherical cathode materials. c) HRTEM image of cathode materials. d) Schematic diagram of electron migration through hierarchical structure. Reproduced with permission.[18b] Copyright 2014, American Chemical Society. e) DFT calculation of the adsorption energy of ethanol molecules on different terminal surfaces. f) Orthogonally arranged nanoplates induced by the ethanol. g–k) SEM images of carbonate precursor with different content of ethanol. Reproduced with permission.[18c] Copyright 2017, American Chemical Society.

improving surface stability, and greatly facilitated the conduction of electrons in the primary particles (Figure 3d). Due to the simple chemical treatment, the activation problem associated to the large primary particles was solved. Finally, the excellent long-term energy retention of up to 93% after 600 cycles was achieved. This unique engineering method can achieve a balance between constructing an ideal structure and achieving effective activation. The inevitable volume change of the spherical secondary particles during the insertion and extraction of lithium ions will cause irreversible structural changes, which greatly hinders the further application. It is proposed that the stability of the local structure can be enhanced by adjusting the microstructure. Specifically, grain refinement and adjustment of the primary particle shape can be applied to suppress internal strain in the high-charge state, thereby suppressing the formation of microcracks during cycling. According to thermodynamics, the growth of a certain crystal plane is closely related to its surface free energy. Xu et al.[18c] chose transition metal carbonate as the precursor, combined with first-principles calculations to synthesize orthogonally arranged nanoplate structures. It was shown in Figure 3e that ethanol molecules had a strong tendency to be adsorbed on the (001) surface of the precursor. Transition metal ions reacted with CO_2 to form precipitates, which gradually nucleated and grew into particles in Figure 3f. With the increase of ethanol content, the obtained precursors gradually changed from microspheres to orthogonally arranged nanoplates to flower-shaped architecture (Figure 3g–k). The specific orthogonally arranged Li-rich layered oxide nanoplates maintained the best cycle and rate capability owing to the anisotropic Li^+ diffusion tunnels.

Moreover, numerous studies have made efforts to reveal a more direct connection between dimensions and performance by the electrochemical properties of comparing cathode materials with different dimensions. These structures usually have the same chemical composition and different morphologies through a variety of synthetic methods. For example, Fu et al.[19] constructed $Li_{1.2}Mn_{0.56}Co_{0.12}Ni_{0.12}O_2$ cathode materials with different morphologies, from 1D rod-like structure to 2D plate-like and 3D spherical structures, and tried to reveal the relationship between different structures and electrochemical performance through a systematic study as shown in **Figure 4**. It was found that 1D microrod particles exhibited excellent cycle stability at high rates, which was far superior to the 2D plate and 3D spherical structures. This was attributed to its unique 1D porous layered structure, which was conducive to the rapid transport of lithium ions in the reversible electrochemical process and high structural stability. Also, it was revealed that the polarity of the solvent played an important role in controlling the morphology of the precursor. Actually, for cathode materials with the same composition and different morphologies, the factors that affect their electrochemical performance are diverse. The surface characteristics of cathode materials with different dimensions also exert an important influence on their structural stability and electrochemical performance. In view of this, Cui et al.[7] synthesized $Li_{1.2}Ni_{0.13}Co_{0.13}Mn_{0.54}O_2$ cathode materials with different morphologies through diverse methods, and discussed the relationship between structure and performance from the perspective of surface oxygen vacancies. Theoretical calculations and characterization results showed that the abundant oxygen vacancies on the surface of the cathode material could effectively reduce the energy barrier for lithium-ion migration, thereby greatly promoting the kinetic process. Correspondingly, the prepared 1D rod-like particles delivered an initial discharge capacity of up to 306.1 mAh at 0.1C rate and maintained a capacity retention of 91.0% after 200 cycles at 0.2C rate.

As a special 3D micro–nano structure, the core–shell structure of the cathode material usually exhibits a spherical morphology, which the core layer and the shell layer have different chemical compositions. Compared with 3D spherical particles with uniform chemical composition and element distribution, the core–shell structure can reduce unnecessary interface side reactions with the electrolyte and improve the thermal stability of the structure. This artful and unique structural design provides a good guidance and scientific significance for constructing a high-performance and high-stability dimensional structure. Generally, core–shell structure of the cathode material selects a Ni-rich material with high specific capacity as the core, and uniformly coats the outer layer with a Mn-rich material with high stability as the shell, thereby achieving the synergy of the two components. In order to meet the requirements of cathode materials for the high specific capacity, high structural stability and high thermal stability, Sun et al.[20] proposed a new concept of a core–shell structured cathode material. A material with a higher nickel concentration can provide higher capacity, but the surface is prone to unnecessary side reactions with the electrolyte, resulting in poor interface stability.[20] For the core–shell structure, this structure usually uses a nickel-rich material as the core layer and a manganese-rich material as the shell layer, which can exhibit high capacity while maintaining high thermal stability, as shown in **Figure 5**a. Initially, it is widely used to improve the electrochemical performance of Ni-rich cathode materials and has achieved significant effects. It is well studied that the Ni-rich cathode material owns a higher capacity, but the higher nickel content on the surface is prone to react with the electrolyte at the high-charged state, leading to severe gas production. In order to solve this problem, Sun et al.[20a] first synthesized and reported a microscale core–shell structure as the cathode material, that is, $Li[Ni_{0.8}Co_{0.1}Mn_{0.1}]O_2$ with high capacity was applied as the core layer and $Li[Ni_{0.5}Mn_{0.5}]O_2$ with excellent thermal stability was applied as the shell layer. The core–shell structure could achieve the synergy of high specific

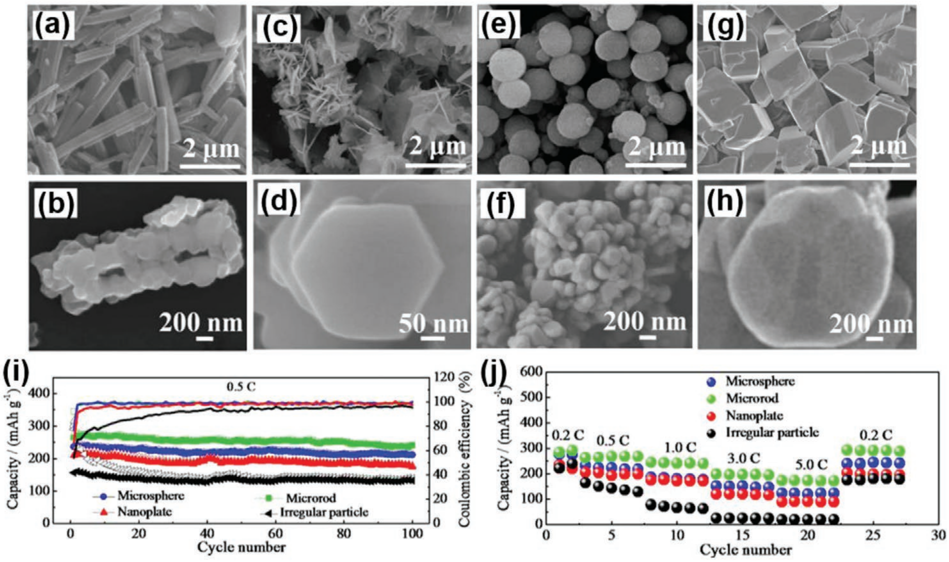

Figure 4. SEM images of the precursor and cathode of microrod a,b), plate c,d), microsphere e,f), and irregular particles g,h). Comparison of the cycle and rate performance i,j). Reproduced with permission.[19] Copyright 2017, Elsevier.

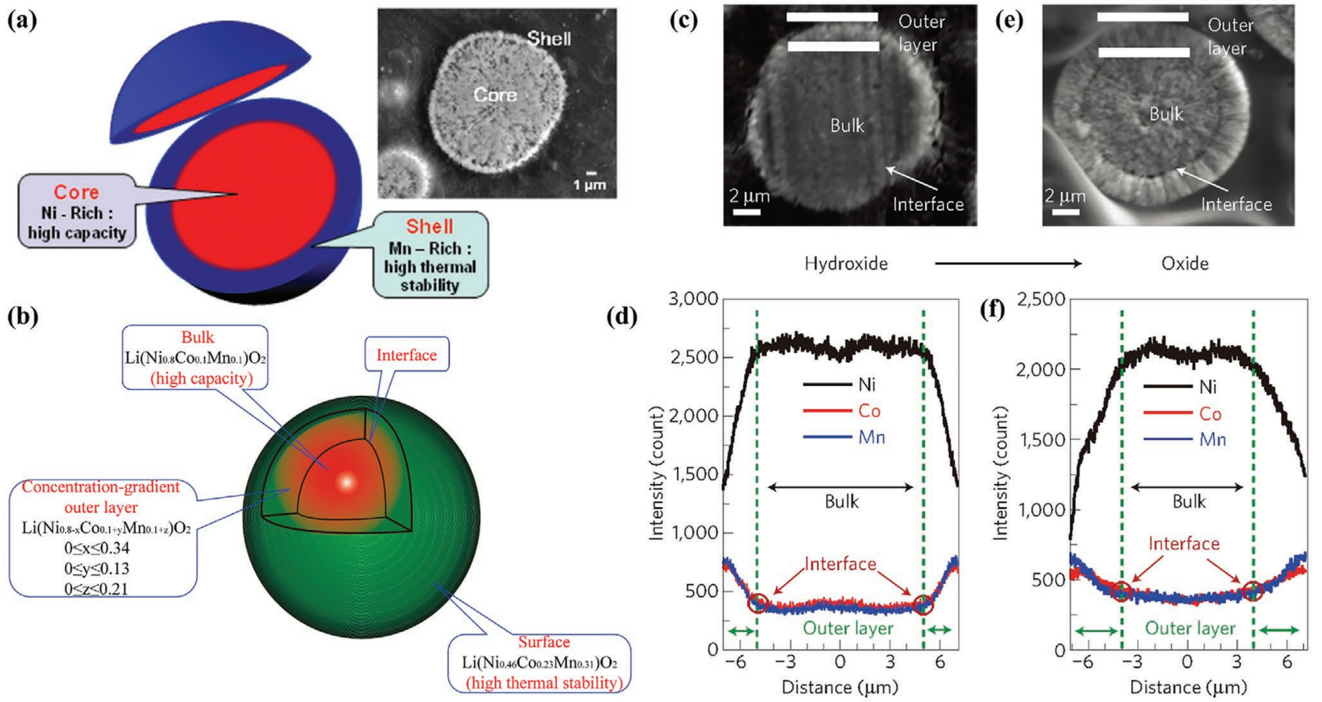

Figure 5. a) Schematic diagram of the core–shell structure and SEM image of core–shell Li[$(Ni_{0.8}Co_{0.1}Mn_{0.1})_{0.8}(Ni_{0.5}Mn_{0.5})_{0.2}$]$O_2$ particle. Reproduced with permission.[20a] Copyright 2005, American Chemical Society. b) Schematic diagram of cathode particles surrounded by a concentration gradient outer layer with a Ni-rich core. c–f) SEM images and EPMA line scan of the hydroxide precursor and lithiated oxide. Reproduced with permission.[20b] Copyright 2009, Nature Publishing Group.

capacity and high thermal stability. As a new type of cathode material, Li[$(Ni_{0.8}Co_{0.1}Mn_{0.1})_{0.8}(Ni_{0.5}Mn_{0.5})_{0.2}$]$O_2$ exhibited a capacity retention record of 98% after 500 cycles, which was of great significance for the development of cathode materials with high energy density and cycle stability. However, the core–shell structure also has inherent shortcomings, especially the serious interface problem. Due to the different volume changes during charge and discharge process, cracks can be easily generated at the boundary between the core layer and the shell layer.

Based on the core–shell structure, a new structure with the characteristics of the concentration gradient aimed at removing the barrier of the structural mismatch is evolved and developed. The full concentration-gradient structure directly connects the end of the Ni-rich core layer with the concentration-gradient Mn-rich shell layer to form a continuous elemental composition change. It can effectively suppress the formation of microcracks at the boundary and simultaneously alleviate the surface reconstruction. Therefore, Sun's group synthesized a new layered lithium nickel cobalt manganese oxide with an average composition of $Li[Ni_{0.68}Co_{0.18}Mn_{0.18}]O_2$.[20b] In this material, each particle utilized $LiNi_{0.8}Co_{0.1}Mn_{0.1}O_2$ as the bulk material surrounded by an outer layer with a concentration gradient in Figure 5b. From the center of the particle to the surface, the Ni concentration gradually decreased, while the Mn and Co concentrations increased (Figure 5c–f). The higher nickel content of the inner layer could satisfy higher energy density, while the increasing manganese content of the outer layer could ensure excellent cycle performance and thermal stability. The half-cell test indicated the core–shell structure with a concentration gradient gained a discharge capacity of 209 mAh g^{-1} and a capacity retention of 96% after 50 cycles under 55 °C. Moreover, they developed a cathode material with a full concentration-gradient structure.[20c] It not only achieved a high overall energy density, but also maintained the unprecedented cycle stability with a capacity retention of 90% after 1000 cycles in a full cell. The Li-rich Mn-based cathode material also takes advantage of the core–shell structure to improve its poor thermal stability and voltage decay. Li et al.[21] designed and synthesized a core–shell structure with 67 mol% of core with the composition $Li_{1+x}(Ni_{0.67}Mn_{0.33})_{1-x}O_2$ and 33 mol% of shell with the composition $Li_{1+y}(Ni_{0.4}Mn_{0.5}Co_{0.1})_{1-y}$. The EDS mapping results showed clear Mn-rich shells, Co-rich shells and Ni-rich cores in the hydroxide precursor. After high-temperature sintering and lithiation process, the obtained cathode material retained the Mn-rich shell, while the Co element was evenly distributed throughout the particles. Compared with samples containing only core or shell components, the $0.67Li_{1+x}(Ni_{0.67}Mn_{0.33})_{1-x}O_2\cdot 0.33Li_{1+y}(Ni_{0.4}Mn_{0.5}Co_{0.1})_{1-y}O_2$ series delivered a reversible initial capacity of 218 mAh g^{-1} with a capacity loss of 30 mAh g^{-1} and a capacity retention of 98% after 40 cycles. Most recently, Wu et al.[22] designed a series of full concentration gradient-tailored agglomerated-sphere Li-rich Mn-based cathode materials through the coprecipitation method. The gradient-tuned Li-rich Mn-based cathode material could inhibit the transformation to a spinel structure during cycling, optimize electrochemical stress and inhibit Jahn–Teller effect. Therefore, it could significantly reduce voltage decay, enhance rate performance, and improve thermal stability. The Li-rich Mn-based cathode material with medium slope gradient showed the best electrochemical performance with a very low average voltage decay of 0.8 mV per cycle. It is worth noting that the precursor should avoid interdiffusion of transition metal ions during the sintering process to maintain its concentration gradient. To be precise, the preparation of the precursor and the sintering process jointly determine the final core–shell structure and concentration-gradient structure. Additionally, the buffer layer can be applied to improve its interface compatibility. From the core–shell structure to the concentration-gradient structure, it is not difficult to find that the composition and element distribution of the cathode material are critical to its electrochemical performance. The strategy of element concentration-gradient adjustment also has important guiding significance for other energy storage materials and electrocatalysis fields.

The composite structure can be obtained by mixing the Li-rich Mn-based cathode material together with a lithium-ion intercalation host material to recapture lithium ions that cannot return to the layered structure, thereby improving the initial Coulombic efficiency. Manthiram's group[23a] took the lead in synthesizing the $Li[Li_{0.2}Mn_{0.54}Ni_{0.13}Co_{0.13}]O_2$-$Li_4Mn_5O_{12}$ composite and $Li[Li_{0.2}Mn_{0.54}Ni_{0.13}Co_{0.13}]O_2$-$LiV_3O_8$ composite through a simple blending method, and found that a certain amount of $Li_4Mn_5O_{12}$ and LiV_3O_8 could both effectively reduce the irreversible capacity loss in the first cycle. This was mainly due to the ability of $Li_4Mn_5O_{12}$ and LiV_3O_8 materials to accept lithium ions extracted from the $Li[Li_{0.2}Mn_{0.54}Ni_{0.13}Co_{0.13}]O_2$ material that were not able to be returned. As a result, an initial Coulombic efficiency of nearly 100% and a high first-cycle discharge capacity of up to 280 mAh g^{-1} have been attained. Afterward, their group also tried to mechanically mix the lithium-free insert VO_2 with Li-rich Mn-based cathode materials and obtained a similar effect.[23b] Besides, Wu et al.[24] utilized a high-energy ball milling process to mix the $Li[Li_{0.2}Mn_{0.54}Ni_{0.13}Co_{0.13}]O_2$ material with the electrochemically active material MoO_3. By analyzing the dQ/dV curves, it was found that MoO_3 could compensate for the lithium sites in the Li-rich layered oxide by providing additional lithium insertion sites. As the content of MoO_3 increased from 0 to 20 wt%, the initial irreversible capacity loss of the composite material decreased from 81.8 to 1.2 mAh g^{-1}.

Whether by designing the morphology and dimensions of the cathode material, or adjusting the atomic concentration gradient from the inter to the outer layer of the particles, researchers are trying to achieve the goal of improving electrochemical performance from the following aspects: i) Nanotechnology can effectively shorten the diffusion path of lithium ions in the primary particles, and the primary particles can expose more Li^+ electrochemically active surfaces, especially the (010) crystal plane, which facilitates the rapid insertion and extraction of lithium ions. ii) Since Ni element can provide higher energy density and average voltage and Mn element helps to enhance structural stability and thermal stability, synergistic effects can be obtained by adjusting the concentration gradient of specific elements. iii) By blending the cathode material with another lithium-ion intercalation host, the lithium ions that cannot return to the cathode layered structure can be recaptured to improve the initial Coulombic efficiency. Other strategies, like surface coating and bulk doping, have also played an important role in improving the electrochemical performance and structural stability.

To understand the structure–performance relationship based on the above results, it is clear that Li-rich Mn-based cathode materials could be designed with different dimensions and morphologies through finding delicate synthesis methods, and some unique structure features are generally helpful for improving structural stability and electrochemical capacity. However, there is actually a lack of generally instructive significance for two key problems: one is what the general regulation mechanism for structures is, and the other is how the unique structures influence exactly the final performance. The former requires a fundamental understanding on crystal nucleation and growth processes for the special Li-rich Mn-based cathode materials, and the latter needs more deep researches extended into both crystal phase level and electrode fabrication, because the final performance is easily affected by so many factors such as grain size, crystal boundary, defect, surface features and electrode texture. Therefore, synthesis and deep research of bulk single crystal materials could be an effective approach to realize dynamics and thermodynamic processes of the unique structured Li-rich Mn-based cathode materials. On the other hand, some typical structures that have been proven relatively stable in cycling by many works from different research groups, e.g., orthogonal, should be carefully investigated common characteristics of crystal including cation mixing and phase transformation.

3. Evolution of Phase Transformation

Most researches have made efforts to promote the kinetic process and thermal stability by constructing cathode materials of different dimensions to achieve the purpose of improving cycle capability and suppressing voltage attenuation. Essentially, the capacity and voltage decay are rooted in the irreversible phase transformation during cycling. Cathode materials of different dimensions have differences in appearance, but in essence, they all belong to a layered structure. Enhancing the stability of the layered structure and reducing the mixing of cations is the essence of constructing structures with different dimensions. Therefore, studying the phase transformation process of the layered structure has important guiding significance for deep understanding of the construction of dimensional structure. Although the influence of dimensionality on the electrochemical performance of cathode materials can be reflected in lithium-ion conduction, electrode process kinetics, and thermal stability, in-depth understanding of the molecular phase transformation process still requires a systematic study toward the microreaction mechanism behind. For example, the morphology and size of the particles on the macro scale can be clearly observed, but the phase composition of the original structure on the molecular level is still in dispute. In the synthesis process of cathode materials, how do sintering process, especially the temperature, affect the phase structure of the precursor? The phase transformation is considered to be closely related to the capacity decay and voltage fading, but when the phase transformation process occurs and how it develops over cycling remains unclear. With the development of state-of-the-art characterization techniques, these problems have gradually gained a clearer explanation. This also helps people gradually change their cognition from a macro- to a microperspective.

The structural formula of Li-rich Mn-based cathode materials can usually be written in three different notations, including $x\mathrm{Li_2MnO_3}\cdot(1-x)\mathrm{LiMO_2}$, $x\mathrm{Li[Li_{1/3}Mn_{2/3}]O_2}\cdot(1-x)\mathrm{LiMO_2}$, and $\mathrm{Li_{1+x}M_{1-x}O_2}$ (M = transition metal).[25–27] Since its emergence, the claims about the phase composition of its original structure have been controversial. Many studies have tried to explain its complex structure by revealing the phase evolution mechanism in the synthesis process. Besides that, the oxygen release due to anionic redox can lead to lattice distortions and defects in microstructure, such as voids inside the particles.[28–31] Additionally, it will further promote the migration of transition metals into lithium sites during cycling, thereby initiating a phase transformation from layered to spinel or even rock-salt phases.[32–34] These processes are closely related to voltage decay and capacity decay, which is also the focus of current research. Herein, the activities on crystal lattices, ionic and atomic levels are discussed to understand what happens to the Li-rich Mn-based cathode materials during charge–discharge process.

3.1. Phase Composition

It is very necessary to understand the lattice structure of Li-rich Mn-based cathode materials, because it will significantly influence the electrochemical performance. In terms of its phase composition, the structure of Li-rich Mn-based cathode materials is usually regarded as a solid solution or a nanoscale composite structure composed of layered $\mathrm{LiMO_2}$ and layered $\mathrm{Li_2MnO_3}$, both of which can be considered as the layered α-$\mathrm{NaFeO_2}$-type rock salt structure.[35–40] The crystal structure models of Li-rich Mn-based cathode materials, $\mathrm{LiMO_2}$ and $\mathrm{Li_2MnO_3}$ are shown in **Figure 6**a,b. In general, $\mathrm{LiMO_2}$ (M = Ni, Co, Mn, etc.) possesses a hexagonal layered structure with the space group of $R\bar{3}m$, and the most typical one is $\mathrm{LiCoO_2}$. And $\mathrm{Li_2MnO_3}$ belongs to the monoclinic layered structure with the space group of $C2/m$. Structurally, these two components are very similar, which also accounts for the complexity of the structure of Li-rich Mn-based cathode materials. Both $\mathrm{LiMO_2}$ and $\mathrm{Li_2MnO_3}$ have a cubic closely packed oxygen arrays, and all octahedral sites are occupied by Li or transition metals. Since $\mathrm{Li_2MnO_3}$ can be written into $\mathrm{Li[Li_{1/3}Mn_{2/3}]O_2}$, it can be understood that lithium ions occupy a third of the transition metal layer. From the X-ray diffraction (XRD) results of Li-rich Mn-based cathode materials, the main diffraction peaks can correspond well to the $R\bar{3}$m space group. And the weak short-range ordered diffraction peak appearing at $2\theta = 20°–25°$ is mainly due to the ordered arrangement of $\mathrm{Li^+/Mn^{4+}}$ superlattices, which can be indexed to the C2/m space group.[41–43] Synchronous X-ray diffraction (SXRD) patterns show that in the range of $2\theta = 6°–8°$, the weak reflections of (020), (110), and (−111)

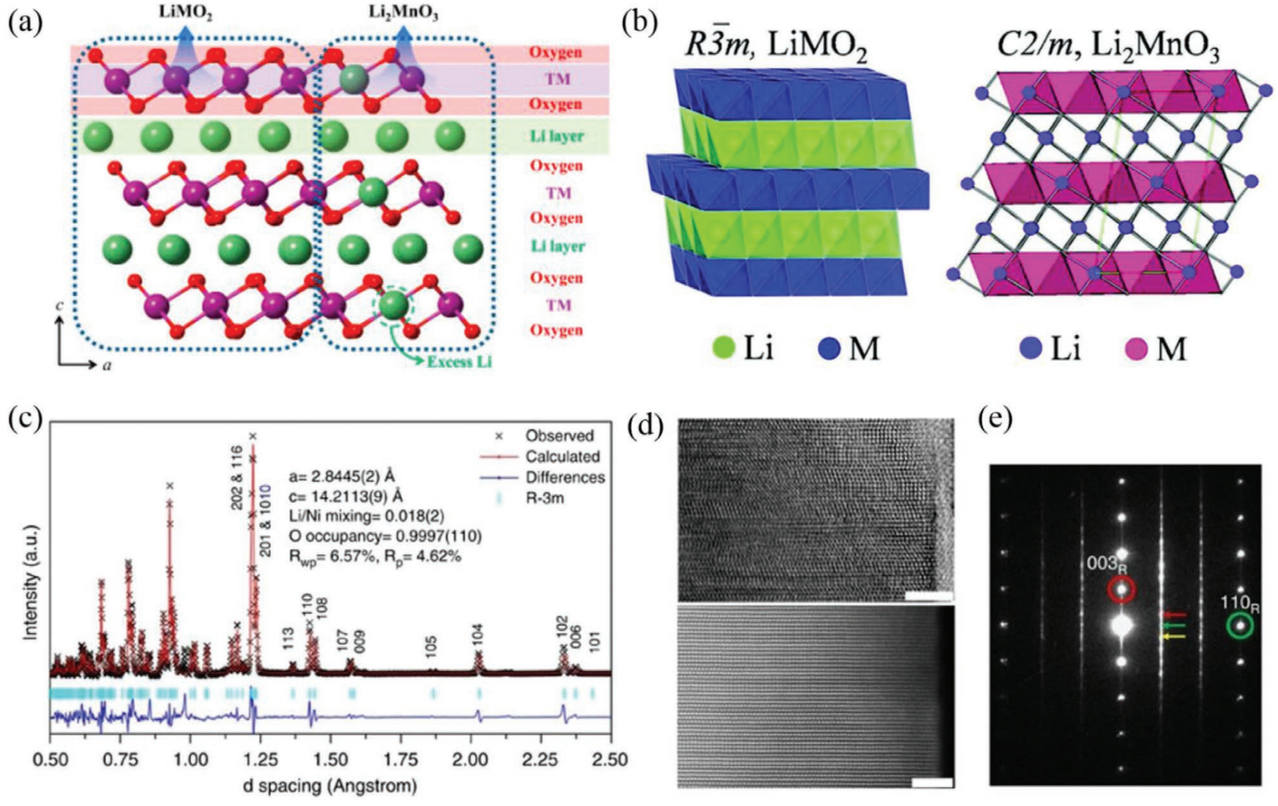

Figure 6. a) Schematic diagram of Li-rich Mn-based cathode materials. Reproduced with permission.[35] Copyright 2015, Elsevier. b) Crystal structure models of $\mathrm{LiMO_2}$ and $\mathrm{Li_2MnO_3}$. Reproduced with permission.[36] Copyright 2015, American Chemical Society. c) Neutron diffraction patterns of pristine $\mathrm{Li[Li_{0.144}Ni_{0.136}Co_{0.136}Mn_{0.544}]O_2}$ materials. d) High-resolution transmission electron microscopy (HRTEM) and high-angle annular dark-field-STEM (HAADF-STEM) image of pristine $\mathrm{Li[Li_{0.144}Ni_{0.136}Co_{0.136}Mn_{0.544}]O_2}$ materials. e) Electron-diffraction (ED) pattern of pristine $\mathrm{Li[Li_{0.144}Ni_{0.136}Co_{0.136}Mn_{0.544}]O_2}$ materials. Reproduced with permission.[46] Copyright 2016, Nature Publishing Group.

lattice planes correspond to the monoclinic Li_2MnO_3 phase of the $C2/m$ space group in the Li-rich Mn-based cathode material. However, the XRD results reflect more on the average crystal structure. More advanced characterization techniques are needed to better understand the pristine phase composition of Li-rich Mn-based cathode materials.

In order to gain more direct evidence, many advanced instruments such as time-of-flight Neutron diffraction (TOF ND) patterns, high-resolution transmission electron microscopy (HRTEM) combined with electron energy loss spectroscopy (EELS), aberration-corrected scanning-transmission electron microscopy (STEM), and high angle annular dark field scanning transmission electron microscopy (HAADF-STEM) have been used to excavate structural information. There are two main standpoints about the phase composition of Li-rich Mn-based cathode materials. One standpoint is that it is a solid solution containing both $LiMO_2$ and Li_2MnO_3 components, which obeys Vegard's law. For example, Storey et al.[44] first reported a new series of layered manganese oxide cathodes of $Li_{2+x}Cr_yMn_{2-y}O_{4+\delta}$, which were ascribed to the solid solution. It was demonstrated that the layered structure could be considered as a solid solution of Li_2MnO_3 and $LiCrO_2$ by focusing on $Li_{1.2}Cr_{0.4}Mn_{0.4}O_2$. In addition, Jarvis et al.[45] used a combination of diffraction scanning transmission electron microscopy (D-STEM), aberration-corrected scanning transmission electron microscopy (STEM), and STEM computer simulations, for the first time, to show $Li[Li_{0.2}Ni_{0.2}Mn_{0.6}]O_2$ formed a solid solution at the atomic level. According to their results, this material belonged to the $C2/m$ symmetry. Compared with X-ray diffraction (XRD), neutron diffraction technique (ND) is more sensitive to light elements, especially Li and H elements. In Figure 6c, TOF ND patterns with Rietveld refinement conducted by Meng's group not only calculated the detailed unit cell parameters of Li-rich Mn-based cathode materials, but also accurately obtained the amount of oxygen vacancies in its particles.[46] Furthermore, the ND results demonstrated that the sample was a solid solution of $LiTMO_2$ ($R\bar{3}m$) phase and Li_2MnO_3 ($C/2m$) phase. Besides, the HRTEM, HAADF-STEM, and ED images also exhibited $R\bar{3}m$ symmetry as shown in Figure 6d,e. On the other hand, many studies support the standpoint of nanocomposite structure proposed by Thackeray et al.,[27] which means that the Li_2MnO_3-like and $LiMO_2$-like nanodomains result in short-range order rather than a full solid solution. It was revealed in their study that the structure of $xLi_2MnO_3\cdot(1-x)LiMO_2$ materials consisted of nanometer regions similar to Li_2MnO_3 and $LiMO_2$, confirming the composite properties of these materials. An important reason to support this view is that the Li ions in the transition metal (TM) layer of Li-rich Mn-based cathode materials are not enough to maintain the ratio of 1Li/2TM found in Li_2MnO_3. This also explains why several studies find evidence of nanodomains composed of both Li_2MnO_3-like and $LiMO_2$-like components. Yu et al.[47] applied atomic-resolution scanning transmission electron microscopy (STEM) to provide strong evidence for the intergrowth of a rhombohedral $LiMO_2$ structure and a monoclinic Li_2MnO_3 structure coexisting in the studied $Li_{1.2}Mn_{0.567}Ni_{0.166}Co_{0.067}O_2$ material. More precisely, the domains with these two phases were separated by the $(001)_{rh}/(103)_{mon}$ plane along the $[001]_{rh}/[103]_{mon}$ direction, which strongly proved the local structural changes of Li-rich Mn-based cathode materials. The controversy about the composition structure of Li-rich Mn-based cathode materials is likely to continue, because various factors including Li content, sintering rate, elemental composition, and synthesis temperature will affect it.

The overall performance of Li-rich Mn-based cathode materials is closely related to its phase composition and synthetic process. Based on the existing evidence, we are more inclined to believe that the Li-rich Mn-based cathode material is formed by the alternating growth of Li_2MnO_3 and $LiMO_2$ nanodomains, rather than a uniform single phase. The inevitable involvement of oxygen release, atomic rearrangement and transition metal ion reduction during heat treatment cause the complexity of its phase composition. Therefore, in order to obtain a cathode material with excellent performance, it is necessary to design a material with a fine layered structure. Also, the calcination process is very important to its phase composition. It is proposed that the heat treatment process should maintain thermal uniformity, fast and efficient thermal process and low heating budget. In addition, the phase composition of the surface and bulk phase of the Li-rich Mn-based cathode material may be different. The spinel phase is more likely to exist on the surface. Therefore, optimizing the phase composition of its surface structure may be of great significance for improving the stability of its overall structure.

3.2. Microstructural Changes

As for Li-rich Mn-based cathode materials, where and how the microstructural changes caused by stress and strain occur and evolve have not been thoroughly studied or elaborated. Furthermore, the reversible anionic reaction in the bulk can also influence the local structure, promote transition metal movement and trigger transformations based on strain and crystal defects. In order to observe the pore formation and structural change of Li-rich cathode materials during the electrochemical process, Hu et al.[48] conducted atomic resolution annular dark field STEM imaging (ADF-STEM), space-resolved electron energy loss spectroscopy(EELS) and ADF-STEM tomography imaging technique to reconstruct the 3D internal structure of $Li_{1.2}Ni_{0.15}Co_{0.1}Mn_{0.55}O_2$ particles in the pristine state and after 15 cycles. As shown in **Figure 7**b, it was clear to see that a new large pore group was formed inside the cycled particles (15 cycles) from the qualitative analysis results of 3D reconstruction in contrast to the pristine sample (Figure 7a). By comparing the pore size distribution (Figure 7c–f), it could be inferred that the new large pores formed during cycling were closely related to the irreversible oxygen loss process, which left nucleating vacancies on the surface of particles. Tran et al.[49] proposed before that oxygen ions would migrate from the bulk to the surface under the formation of oxygen vacancies, while transition metal ions migrated from the surface to the bulk as a result of lattice densification. It is worth noting that the subsequent differential electrochemical mass spectrometry (DEMS) test results detect the oxygen release in the form of O_2 under high charging potential. In order to further illuminate the formation nature of pores during cycling, it is speculated that the newly generated

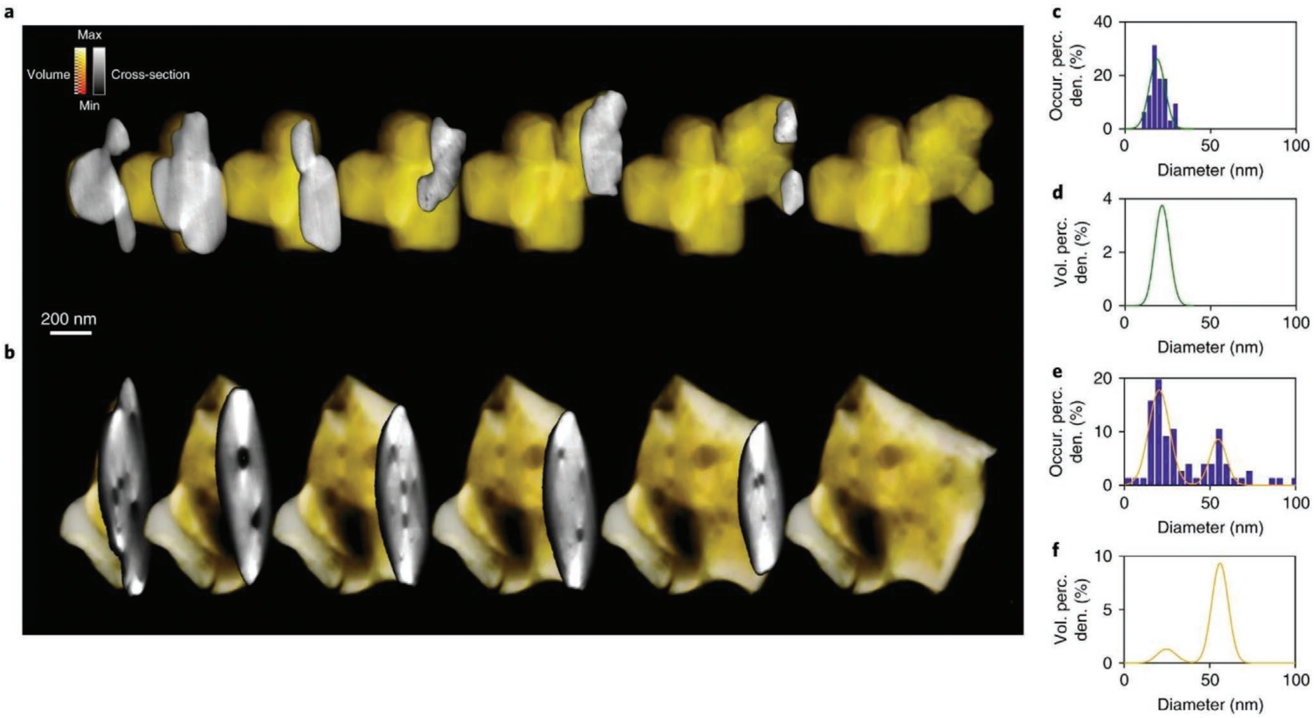

Figure 7. 3D electron tomography results of $Li_{1.2}Ni_{0.15}Co_{0.1}Mn_{0.55}O_2$ cathode materials. a,b) Volume renditions and progressive cross-sectional images of particles in the pristine sample and after 15 cycles. c,d) The size distribution of internal pores generated in the pristine cathode weighted according to occurrence and volume, respectively. e,f) The size distribution of internal pores generated in the cathode after 15 cycles weighted according to occurrence and volume, respectively. Reproduced with permission.[48] Copyright 2018, Nature Publishing Group.

pores are neither entirely concealed in the bulk phase of particles, nor entirely exposed on the surface of the electrolyte and particles. On the contrary, they tend to accumulate in the vicinity of oxygen diffusion channels in the form of microstructural defects, such as dislocations, cracks, etc., and then with the increase in size and number, further promote microstructural changes, and ultimately accelerate oxygen loss and voltage decay. Moreover, Li et al.[50] studied two different types of crystalline defects in Li_2MnO_3 during the delithiation stage and oxygen activity by applying in situ high-resolution transmission electron microscopy (HRTEM) combined with density functional theory (DFT) calculations. On one hand, stacking faults might be related to the reversible anionic redox due to the lower activation energy. On the other hand, dislocations were likely to generate at a higher potential and assist oxygen atoms to transfer to the surface of particles, and thus evolve with irreversible oxygen loss.

Additionally, Yan et al.[51] also confirmed that nanovoids were created in the bulk of particles by using 3D tomographic reconstruction technology to visualize the formation of nanovoids during cycling. It not only showed the spatial distribution of nanovoids, but also revealed the lattice reconstruction and mass loss due to the formation of nanovoids. In order to further understand how nanovoids propagate and evolve in a single particle, STEM-HAADF imaging was conducted to track the nanovoid-populated area. Through successive observation of $Li_{1.2}Mn_{0.6}Ni_{0.2}O_2$ cathodes with different cycles, it could be seen that the formation of nanovoids started from the surface of the particles, and gradually propagated and expanded to the bulk phase over cycling. As shown in **Figure 8**, the thickness of the degradation layer associated with nanovoids gradually increases with the increase of cycle number. After 45 cycles, disordered region appears in the interior of the pristine layered structure, which is inseparable from cation mixing. In the long cycling, some smaller particles even suffer from severe structural degradation due to a higher nanovoid density. Corresponding composition analysis shows that the formation of nanovoids is accompanied by oxygen release and lithium depletion under a high charge potential. The formation and evolution process of nanovoid-populated area indicates the injection of oxygen vacancies from the particle surface into the bulk lattice during cycling. Previous studies have also reported that this activation process promoted the migration of transition metal ions into the lithium layer, exacerbating structural degradation.[52–56] This provides a new view for understanding the relationship between anionic redox behavior and lattice structure transformation.

3.3. Phase Transformation during Synthesis

It is well known that the phase composition and pristine structure of Li-rich Mn-based cathode materials are complex, and its most widely accepted structural formula is: $x\mathrm{Li[Li_{1/3}Mn_{2/3}]O_2}\cdot(1\text{–}x)\mathrm{LiMO_2}$, of which $Li[Li_{1/3}Mn_{2/3}]O_2$ can be written as Li_2MnO_3. Among them, Li_2MnO_3 component corresponds to the monoclinic phase (space group of C2/m), and $LiMO_2$ component where M is usually a 3d transition metal belongs to the hexagonal structure(space group of $R\bar{3}m$). In order

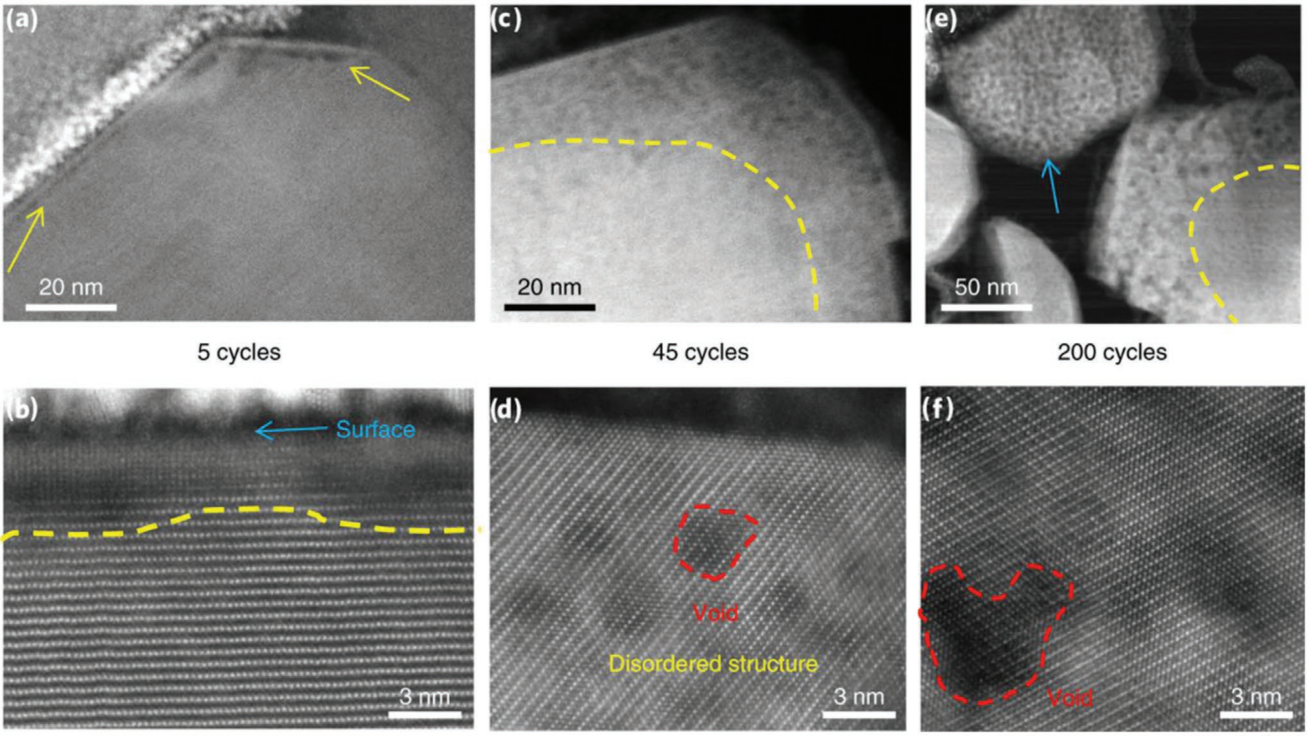

Figure 8. Nanovoid distribution of $Li_{1.2}Mn_{0.6}Ni_{0.2}O_2$ cathode materials in different cycles. The STEM-HAADF images represent the gradual evolution of nanovoid-populated region from the surface to the bulk of particles over cycling. a,b) After 5 cycles. c,d) After 45 cycles. e,f) After 200 cycles. Reproduced with permission.[51] Copyright 2019, Nature Publishing Group.

to gain more phase information, it is essential to study the phase transformation during the synthesis process. Unfortunately, the original phase formation and transformation mechanism of the composite structure of Li-rich Mn-based cathode materials during synthesis have not been fully elucidated, and its electrochemical performance is often closely related to the preparation procedure. Therefore, it is very important to explore the relationships of structure-based lithiation reaction, oxygen incorporation and phase transformation in the calcination process. Hua et al.[57] studied the phase transformation mechanism of $Li[Li_{0.2}Ni_{0.2}Mn_{0.6}]O_2$ cathode materials during the synthesis process via a microwave heating method. In the study, hydroxide precursors were synthesized by the coprecipitation route and Li_2CO_3 was selected as lithium source. By utilizing in situ high-temperature synchrotron radiation diffraction technology to track the phase transformation of the lithium-free hydroxide precursor during heating, it was found that it was impossible to obtain a layered structure only by heating the precursor without a lithium source (**Figure 9**a). After mixing with the lithium source, the initial precursor was dehydrated under high temperature to form a cubic spinel phase (*Fd*-3*m*). When the temperature rose to 550 °C, it gradually transformed into a rock salt phase (*Fm*-3*m*) and two different types of layered phases (*C*2/*m* and *P*3*m*1), and these two different layered phases were formed on the surface of the crystal in contact with the lithium source in Figure 9b. After the temperature reached 740 °C, all of them were converted into a monoclinic layered phase (*C*2/*m*) and a rock salt phase. Driven by the lithium-ion concentration gradient, lithium ions behaved a strong tendency to enter the interior of the crystal, reflecting the instability of the overlithiated structure in the reaction system. At a higher temperature (up to 840 °C), the rock salt phase eventually formed a monoclinic layered phase, which lithium ions and transition metal ions were arranged at different atomic ordering. Besides, it pointed out that lithium and oxygen gradually entered the spinel skeleton formed by the precursor as the microwave heating temperature increased, thereby continuously forming the rock salt phase until finally forming a layered phase as shown in Figure 9c. This provides a significant theoretical basis for understanding the effect of lithium–oxygen incorporation on the phase transformation during synthesis and the original structure of the Li-rich Mn-based cathode material. Moreover, it also provides important guidance for optimizing the synthesis path and sintering process of Li-rich Mn-based cathode materials.

Not only that, Hua et al.[58] also revealed the dependence of the phase transformation on the lithium content in the synthesis process through a systematic research of $Li[Li_{0.2}Ni_{0.2}Mn_{0.6}]O_2$ cathode material. According to a series of thermodynamic studies on the $Li_xNi_{0.2}Mn_{0.6}O_y$ ($0.00 \le x \le 1.52$), it is disclosed that it appears as a thermodynamically stable cubic spinel phase with the space group of *Fd*-3*m* at a lower lithium concentration ($0.00 \le x < 0.40$). Lithium ions are inserted into tetrahedral sites of the host structure in this stage. As the lithium content further increases ($0.40 < x < 1.20$), there will be a region where three phases coexists: a Li-poor spinel phase with the space group of *Fd*-3*m*, a Li-containing rock salt phase with the space group

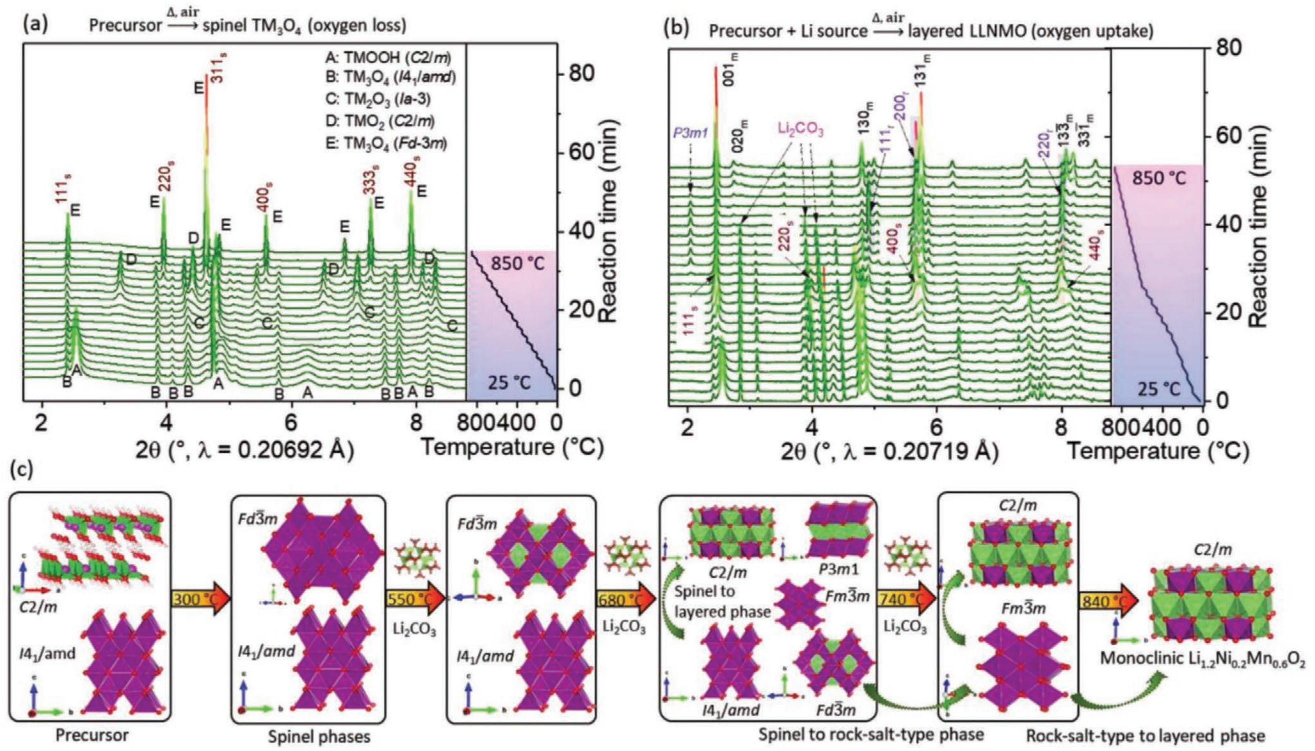

Figure 9. The results of in situ high-temperature synchrotron radiation diffraction of a) Li-rich precursor. b) Li-rich precursor with Li_2CO_3 (lithium source). c) Schematic diagram of the phase evolution when the precursor reacts with Li_2CO_3 at high temperature. Reproduced with permission.[57] Copyright 2019, Wiley-VCH.

of *Fm*-3*m*, and a Li-rich layered phase with the space group of *C*2/*m*. More specifically, the percentage of the layered phase accounts for 82% when the *x* increases to 1.20, which indicates a gradual transformation toward layered structure. More and more lithium ions are going to lie in the octahedral sites, taking part in the formation of the layered and rock salt phase. After the lithium content exceeds the predetermined value of 1.2, all other nonlayered phases will be converted into the layered structure. Synchronous diffraction results show that most of the diffraction peaks correspond to the rhombohedral phase with the space group of $R\bar{3}m$ and some weak diffraction peaks belong to the monoclinic phase with the space group of *C*2/*m*. The analysis of cathode materials cycled for 373 days revealed that pristine layered structure transformed to Li-poor spinel phase and disordered rock salt phase, which was mainly due to the release of Li_2O at high potential over long cycling. As shown in **Figure 10**, a surface-bulk-limited reaction is proposed to explain the formation mechanism of Li-rich Mn-based cathode materials. During the rapid heating process, the Li-free spinel phase will be completely transformed into a disordered rock salt phase due to insufficient reaction time for cation ordering. Under high-temperature conditions, the activation energy barrier of the transformation from rock salt-containing intermediates to Li-rich cathode materials can be easily broken through, but at room temperature, this activation energy barrier can hinder the thermodynamic phase transformation. This also explains why the layered structure is more likely to transform into Li-poor spinel phase or even rock salt phase in the loss of Li_2O over long cycling.

3.4. Phase Transformation during Cycling

The irreversible phase transformation from the layered structure to a new phase due to oxygen loss and Li/Ni mixing of the Li-rich Mn-based cathode material during cycling will not only seriously affect its structural stability, but also be an important cause of voltage decay and capacity fading. Although the mechanism of phase transformation in long cycling has not been fully understood, this new phase is commonly represented as a spinel-like phase. Previously, numerous studies have provided direct evidence of the expanding spinel-like phase domains with the help of state-of-the-art techniques.[59–63] Gu et al.[59] applied STEM-HAADF to study the formation of spinel phase domains of Li-rich Mn-based cathode material after 60 cycles. As shown in **Figure 11**a, two sets of clear lattice fringes indexed to the planes (001) and (111) of the spinel phase have been found, and most of the spinel domains are distributed in the entire particles with nanometer sizes (not only distributed on the surface, but also in the bulk). In addition, these new spinel regions are disorderly arranged and have different orientations from each other (Figure 11b–c). The Fourier transform image also shows that the layered cathode material matrix exhibits a certain degree of collapse, and its lattice is decomposed into polycrystalline and amorphous regions (Figure 11d). By comparing the STEM-EDS mapping results of the original material and the sample after cycling, it is found that cracks exist in the cycled particles. Extensive researchers have reported before that oxygen and lithium ions would extract from Li_2MnO_3 component in the form of Li_2O after being activated under high potential

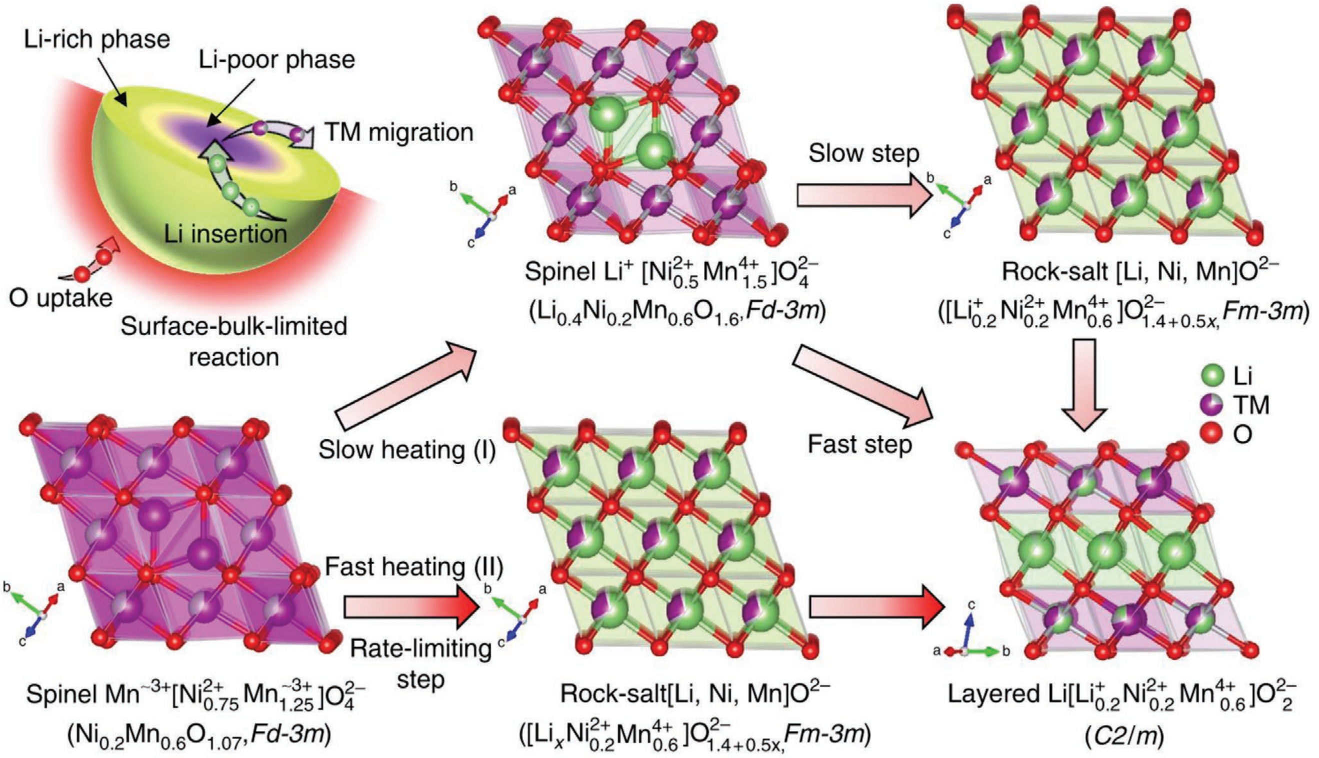

Figure 10. Schematic diagram of two different paths for the synthesis of Li-rich Mn-based layered oxides from Li-free spinel oxides. Reproduced with permission.[58] Copyright 2019, Nature Publishing Group.

condition. These cracks are mainly caused by the movement of metal cations during charging and the strain caused by the collapse of the lattice. It is generally believed that the transition metal ions located at the octahedral site of the metal layer move to the empty octahedral site at the lithium layer through a tetrahedral site. To summarize the phase transformation characteristics of Li-rich cathode materials, Gu et al.[59] concluded that the transition metal ions in $LiMO_2$ migrated to the lithium layer to form a spinel phase similar to $LiMn_2O_4$-type, while Li_2MnO_3 phase appeared amorphous and disordered due to oxygen loss and structural degradation in Figure 11e. The layered-to-spinel phase transformation process usually follows a nucleation and growth mechanism and seriously affects its structural stability, which is an important cause of a reduced energy density.

However, there is still controversy about the origin of the phase transformation in the cycling process, especially whether it starts from the surface or the bulk phase. According to the analysis results, most of studies tend to believe that the phase transformation starts at the surface and then continuously diffuses into the bulk phase during cycling. For example, combining XANES and full-field TXM, Yang et al.[64] investigated the Mn K-edge absorption results of the pristine and cycled $Li_{1.2}Mn_{0.525}Ni_{0.175}Co_{0.1}O_2$ materials to uncover the structural degradation mechanism under high potential. The changes of Mn chemistry during cycling led to the reduction of Mn and formation of spinel, starting from the surface and then gradually processing inward. Yan et al.[56] found that Ni ions migrated from the bulk lattice to the particle surface through a study of the elemental composition evolution of $Li_{1.2}Ni_{0.2}Mn_{0.6}O_2$ cathode materials during cycling, leading to the depletion of Ni content in the bulk lattice and the thickening of the Ni-rich surface reconstruction layer (SRL). In addition, Ni ions were almost depleted on the outermost surface of the SRL and displayed concentration partitions in the SRL thin layer of the cycled sample, which indicated that Ni ions preferentially dissolved in the electrolyte. Due to the migration of Ni from the bulk to the surface and the surface aggregation of Mn, the SRL layer was determined to be a transition metal-rich and lithium-poor phase. Therefore, a sequential phase transformation from the layered to spinel structures occurred on the particle surface, which resulted from the continuous enrichment of transition metal ions and the depletion of lithium ions. In view of this, a number of studies are devoted to adopting the direct method of surface modification to control oxygen activation and prevent structural degradation.[65–68] Liu et al.[69a] conducted a surface doping of Nb on the surface of $Li_{1.2}Mn_{0.54}Ni_{0.13}Co_{0.13}O_2$ materials to improve the electrochemical performance and enhance the structural stability. DFT calculations revealed the doped ions were located in the lithium layer and the stronger Nb—O bonding could weaken the energy overlap between 3d transition metal and O to stabilize the surface structure. Wu et al.[69b] also investigated the effect of surface modification with Al_2O_3, CeO_2, ZrO_2, SiO_2, ZnO, and $AlPO_4$ on the Li-rich Mn-based cathode material. And it was discovered that Al_2O_3 and $AlPO_4$ were the most effective coating materials in maintaining more oxide ion vacancies and prohibiting structural degradation. The in situ formation of LiF decoration on Li-rich Mn-based cathode material can accelerate the diffusion of lithium ions

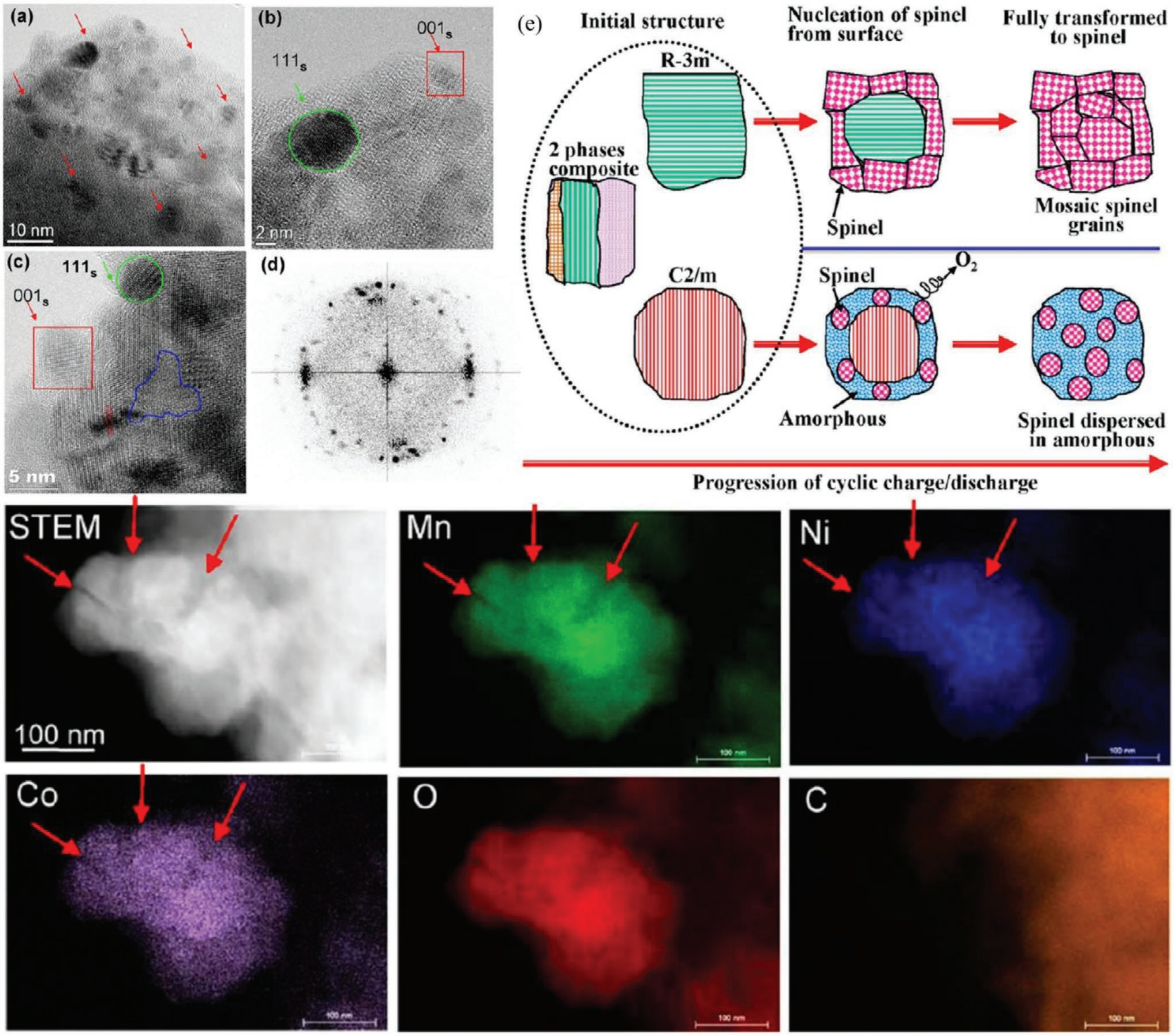

Figure 11. a–c) TEM images of the spinel domains found in the Li-rich Mn-based cathode materials after 60 cycles. d) Corresponding FFT result of TEM image showing polycrystalline diffraction. e) Schematic diagram of the transformation path of the Li-rich layered structure to the spinel structure during cycling. STEM and EDS mapping results show the formation of cracks in the cycled materials. Reproduced with permission.[59] Copyright 2013, American Chemical Society.

and inhibit the layer-to-spinel phase transformation, thereby obtaining superior low-temperature performance.[69c] Overall, the harmful phase transformation of Li-rich Mn-based cathode materials can be effectively suppressed by increasing the stability of the surface and bulk structure, thereby improving the electrochemical performance.

Essentially, Li-rich Mn-based cathode materials with any dimensionality possess layered structure, however, the complexity of their phase composition and lattice matching exacerbates difficulty of studying the phase transformation during cycling process. As presented above, the advanced in situ characterization techniques, especially in situ transmission electron microscopy and synchrotron X-ray diffraction techniques are very powerful for understanding the phase transformation in depth. Furthermore, it is anticipated that more in situ electrochemical technologies and more advanced theoretical simulations based on big data and machine learning can be used to study the promising cathode materials at the lattice level. Significantly, the phase transformation could be directly related to the preparation conditions. For instance, the sintering process has strong influence on the phase composition and the degree of cation mixing, and the optimization of sintering temperature and selection of precursors can help maintain a fine layered structure and inhibit the mixing of cations during the synthesis process. In addition, most of the current studies support that the phase transformation starts on the surface of the electrode material and then gradually diffuses to the bulk phase during cycling. During the charging and discharging process, the vacancies generated on the surface, Jahn–Teller distortion and stress-strain can also cause partially phase change. Especially oxygen vacancies generated on surface of cathode materials may promote the migration of transition metal cations to the lithium layer, which will aggravate the phase transformation process. How to reduce the generation of oxygen vacancies in the electrochemical process should be one of the effective ways to inhibit the phase transformation.

4. Anionic Redox Activity

The phase transformation is closely related to the voltage and capacity decay of the cathode material during the charge and discharge process, and the anionic redox activity plays an important role in the phase transformation and extraordinary capacity. The complexity of anionic redox activity of Li-rich Mn-based cathode materials lies not only in the reversible anionic redox reaction, but also in the irreversible oxygen loss. Moreover, the generation stages and processes of these two parts are also different. It is generally believed that the reversible anionic redox reaction is the main cause accounting for the ultra-high discharge specific capacity, and the irreversible oxygen loss is closely related to the serious capacity decay and phase transformation. Although the discussion on the source of the anomalous capacity of Li-rich Mn-based cathode materials continues, such as the release of O_2,[70] peroxo-like $O_2{}^{n-}$ species,[71,72] proton insertion hypothesis,[73] the formation of oxygen vacancies accompanying $Mn^{2+}/Mn^{3+}/Mn^{4+}$ redox[74,75] and the manganese oxidation of Mn^{+4}/Mn^{+7},[76] here we mainly elaborate on the latest progress about the anionic redox mechanisms that have been extensively concerned in recent years.

4.1. Reversible Anionic Redox Reaction

A widely accepted consensus is that the outstanding specific capacity of Li-rich Mn-based cathode materials is achieved by the cations and anions involved in the redox process during charging and discharging. Both transition metal cations and oxygen anions can reversibly participate in the redox activity. Li_2MnO_3 is well known as the most studied and classic Li-rich Mn-based cathode materials due to the particular electrochemical behavior. Many studies have found that Mn^{4+} maintains electrochemical inertness and charge compensation is completed by oxygen oxidation during the delithiation process of Li_2MnO_3.[70–72] Meanwhile, Li^+ and O^{2-} remove from the lattice in the form of Li_2O. It is demonstrated that oxygen redox participates in the first charge process and contributes to the lithium extraction of Li_2MnO_3.[77–80] A series of in-depth researches based on the electrochemical behavior of Li_2MnO_3 is actually to better understand the mechanism behind the reversible capacity exceeding 250 mAh g^{-1} of its derived materials, $x Li_2MnO_3 \cdot (1-x) LiMO_2$. Li-rich Mn-based cathode materials can be regarded as Li_2MnO_3 substituted by other transition metal ions. The difference is that the layered structure modified by Co or other ions becomes more stable and can effectively suppress the structural degradation after activation. Previously, Li et al.[81a] introduced the role of cobalt in cathode materials of lithium-ion batteries, and proposed that nonmagnetic Co^{3+} could alleviate the magnetic frustration and create a stable cathode. Through studying the influence of Co content on the electrochemical performance of $LiNi_{0.8}Co_xMn_{0.2-x}O_2$ (x = 0, 0.05, 0.1, 0.15) cathode materials, Zhong et al.[81b] found that the cycling stability and rate capability were improved with the increase of Co content. It was demonstrated that Co element in Ni-rich cathode materials could effectively reduce the mixing of cations and improve the electronic conductivity of cathode materials, thereby stabilizing the host structure. Most recently, Liu et al.[81c] affirmed the role of cobalt in the rapid capacity and suppression of Li/Ni mixing by the comparison of Co-free and Co-rich Ni-rich cathode materials. However, it was also found that cobalt was more destructive at high potentials, which could easily lead to the generation of intergranular microcracks. The role of cobalt in the Li-rich cathode may be different from that of the Ni-rich cathode due to the complicated composition and structure. Boivin et al.[81d] reported that the introduction of Co into Li_2MnO_3 could suppress the O loss on charging in Li-rich cathode materials. With a systematic research on low-Co Li-rich cathode materials, Ye et al.[81e] revealed that small changes in Co content had little effect on the crystal structure, but played an important role in improving the activation rate of Li_2MnO_3 phase. Actually, no consensus about the role of cobalt in Li-rich Mn-based cathode materials is achieved in the current researches. Also, Li-rich Mn-based cathode materials exhibit more complex electrochemical behavior than Li_2MnO_3, especially during the first cycle. From its unique first charge curve (**Figure 12**a), it is observed that the first charge process can be divided into two stages: a slope less than 4.4 V and a plateau more than 4.4 V. The differential capacity profiles reveal that the capacity of the former process is mainly contributed by the oxidation of transition metal cations (Co^{3+}/Co^{4+} and Ni^{2+}/Ni^{4+}), and the latter process is mainly contributed by the oxidation of oxygen anions. Koga et al.[82] studied the redox of oxygen in the bulk phase of $Li_{1.20}Mn_{0.54}Co_{0.13}Ni_{0.13}O_2$ before, and proposed that oxygen in the bulk phase could reversibly take part in the electrochemical process rather than in the form of oxygen loss. Moreover, Sathiya et al.[71] detected the reversible conversion of $O^{2-}/O_2{}^{n-}$ ($1 < n < 3$) during cycling with the help of electron paramagnetic resonance (EPR) and X-ray photoelectron spectroscopy (XPS).

Among many possible oxygen dimers, the most convictive explanation is the existence of reversible redox reaction of O^{2-}/O^-. According to this hypothesis, the extraction of lithium leads to the decreasing of the nonbonding oxygen p states, thus causing the oxidation of O^{2-} to O^-.[83,84] The application of in situ surface-enhanced Raman spectroscopy (SERS) in lithium batteries provides significant evidence for observing the presence of peroxo O—O bond formation. Through in situ surface-enhanced Raman technology, Li et al.[72] directly visualized of the reversible O^{2-}/O^- redox in lithiation–delithiation process of $Li_{1.2}Ni_{0.2}Mn_{0.6}O_2$ (Figure 12b). After the emergence of the plateau in the first charge, a new peak appeared and increased at the Raman shift of 850 cm^{-1}, and gradually disappeared during the discharge process. This result was also consistent with calculations based on density functional theory (DFT). Furthermore, this reversible process was not only observed in the first cycle, but also detected a similar reversible process in the

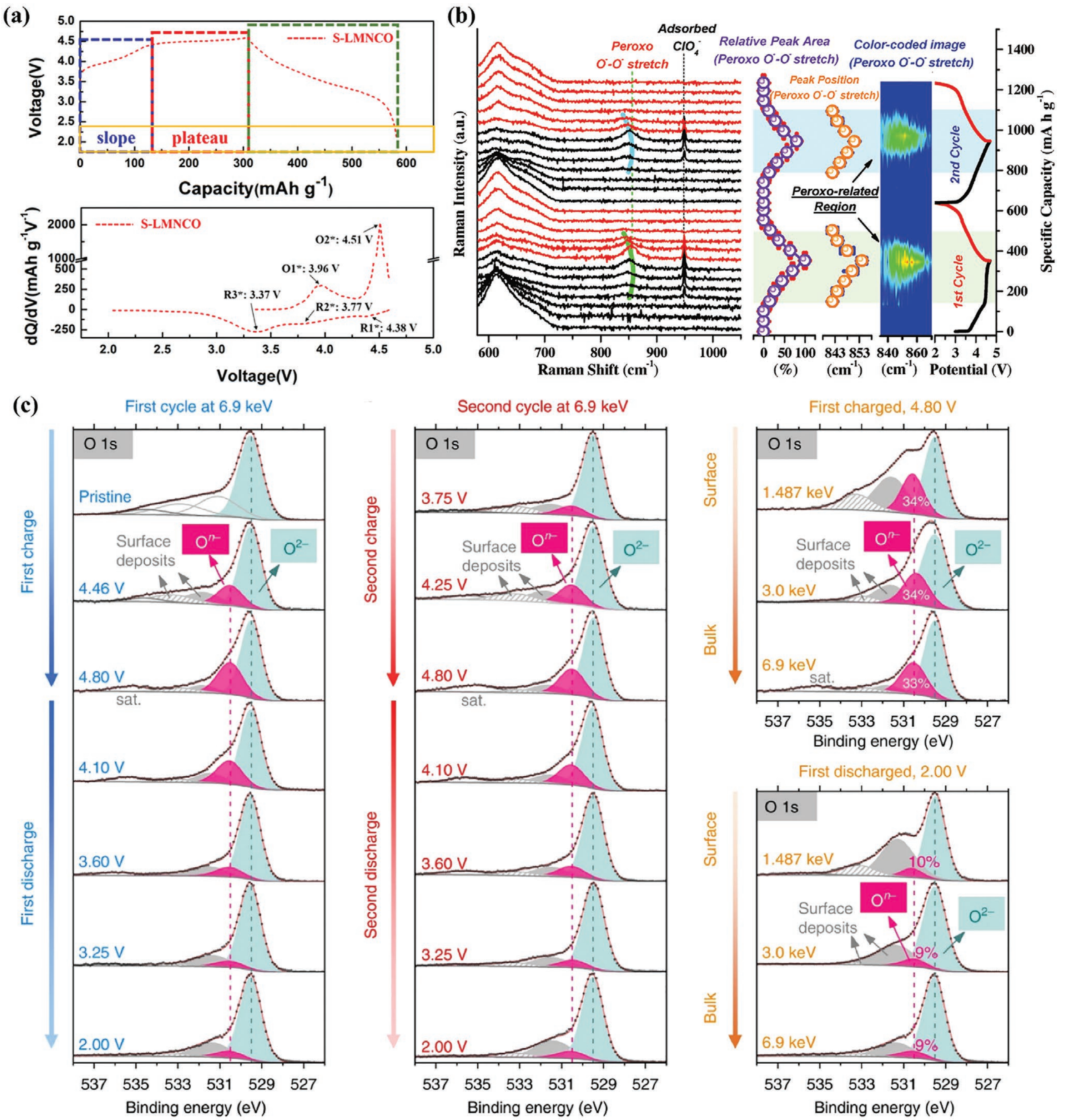

Figure 12. a) First charge/discharge curves and differential capacity profiles of Li-rich Mn-based cathode materials. Reproduced with permission.[80] Copyright 2018, American Chemical Society. b) In situ Raman spectra during the first and second cycles (5 mA g^{-1}). Reproduced with permission.[72] Copyright 2018, Wiley-VCH. c) HAXPES results of O 1s spectra during initial two cycles and of different probing depth. Reproduced with permission.[86] Copyright 2017, Nature Publishing Group.

second cycle. Coincidentally, Zhang et al.[85] conducted a comprehensive study on O$_3$-type Na-rich Mn-based Na$_{1.2}$Mn$_{0.4}$Ir$_{0.4}$O$_2$ cathode materials. An interesting fact was that in situ Raman spectroscopy, soft X-ray absorption spectroscopy (XAS) and X-ray photoelectron spectroscopy (XPS) verified a highly reversible conversion of O^{2-}/O$_2^{2-}$ species in sodium ion cathode materials. Undoubtedly, anionic redox ascribed to O species in Li-rich Mn-based and Na-rich Mn-based cathode materials is of high reversibility. Additional example is that Assat et al.[86] utilized hard X-ray photoelectron spectroscopy (HAXPES) to study the nature of oxygen redox during the first and second cycles. As shown in Figure 12c, a new oxidized O^{n-} ($n < 2$) peak emerges at 530.5 eV when charged to 4.46 V. Then it reaches the maximum after charging to 4.80 V, and gradually weakens until the end of discharge. A similar situation happens in the second cycle. The difference is that the proportion of O^{n-} ($n < 2$) component involved in the form of reversibility in the second cycle is lower than that in the first cycle. After probing two samples (first charged to 4.80 V and first discharged to 2.00 V) at different depths, it is revealed that the intensity and proportion of oxidized O^{n-} are not changed much by the photon energy and probing depth. In addition, it also indicates that O^{n-} exists in the bulk phase. How to make oxygen participate in the reversible redox process in a larger proportion may be a key issue to improve the electrochemical performance of Li-rich Mn-based cathode materials.

4.2. Oxygen Loss

In addition to contributing to the capacity of Li-rich Mn-based cathode materials in the form of reversible redox, a number of studies have found that part of oxygen can bring about severe capacity loss and structural degradation in the form of irreversible oxygen loss. Lu and Dahn[87] first proposed the concept of “oxygen loss” in 2002. The manganese ions of the Li_2MnO_3 component contained in the Li-rich Mn-based cathode materials are already at the chemical state of +4. Therefore, the polarization to high potential will next oxidize the oxygen anions instead of transition metal cations in the compound, resulting in irreversible oxygen loss during the first charge process.[88] In situ differential electrochemical mass spectrometry (DEMS) provides direct evidence for studying oxygen loss by real-time detecting gas composition and recording generation rate in electrochemical reactions. Armstrong et al.[89a] first applied DEMS technique to study the evolution of oxygen gas and proposed that oxygen was evolved from the surface of Li-rich Mn-based cathode materials in the initial charge process. At the plateau stage of the first charge, lithium ions would remove from the octahedral sites in the transition metal layer to the lithium layer through the tetrahedral sites, thereby forming vacancies. The vacant sites were then occupied by the coordinated replacement of transition metal ions that diffused from the surface to the bulk, and this process continued until all octahedral sites vacated by the lithium ions were occupied by transition metals. However, the lithium ions extracted from the first charge could not all return to the original sites during the discharge process, which accounted for a low initial Coulombic efficiency. Gas release is also very important for the study of safety aspects of cathode materials.[89b] Because molecular oxygen easily reacts with the conductive agent and binder of the composite electrode, and accelerates its failure. By establishing a unified model of intermediate peroxo/superoxo-like dimers, Chen et al.[89c] proposed that alleviating oxygen release could help to construct safe and efficient Li-rich Mn-based cathode materials. To evaluate safety, Yamano et al.[89d] introduced a cell design using a Li-rich layered oxide cathode and a SiO–Si composite anode, which did not require a Li predoping process. The safety performance tested by the nail penetration showed that the cell using a Li-rich layered oxide cathode and a SiO–Si composite anode could be used in practical applications.

Moreover, the lattice oxygen release of Li-rich Mn-based cathode materials during cycling can affect its unit cell structure. The in situ X-ray diffraction (XRD) is employed to observe the crystal structure changes by calculating unit cell parameters, so as to realize the real-time detection of the microstructure changes in the electrochemical process. As shown in **Figure 13**a, in the region of voltage slope which is less than 4.4 V, the electrostatic repulsion between two adjacent oxygen layers increases due to the constant extraction of lithium ions from the lithium layer, so that the cell parameter c shows an upward trend. On the contrary, the cell parameter a/b shows a downward trend because of the shrinkage of the radius of Ni/Co cations. In the following plateau stage over 4.4 V, some of oxygen anions are evolved in the form of irreversible oxygen loss, which causes a certain degree of collapse of the crystal structure. The cell parameter c starts to decrease and reach the lowest value at the end of first charge. Moreover, from the change of volume of the entire unit cell, the crystal structure of cathode materials exhibits breathing-like contraction and expansion during the delithiation and lithiation process. Previously, Zhang et al.[90] reported a strategy of spinel $Li_4Mn_5O_{12}$ coating to diminish the lattice oxygen release from the surface of Li-rich Mn-based cathode materials. It was identified that the uniform epitaxial heterostructure coating was favorable to prevent the lattice oxygen removing from the fragile layered framework, thus increasing structural stability.

Bruce’s group[91] used isotope labeling to prepare ^{18}O-labeled $Li_{1.2}[Ni_{0.13}{}^{2+}Co_{0.13}{}^{3+}Mn_{0.54}{}^{4+}]O_2$ cathode materials by heating compounds in $^{18}O_2$-containing atmosphere to achieve ion exchange, and combined with operando differential electrochemical mass spectrometry (DEMS) to analyze the formation of O_2 and CO_2 (Figure 13b). It not only confirmed that O_2 gas began to evolve at and above the charging plateau of 4.5 V in the first charge, but also the generated O_2 gas originated from the lattice of cathode materials, rather than the oxidation of the electrolyte. Besides, through the analysis of generated CO_2 gas, it was found that oxygen atoms escaping from the lattice of $Li_{1.2}[Ni_{0.13}{}^{2+}Co_{0.13}{}^{3+}Mn_{0.54}{}^{4+}]O_2$ materials interacted with the electrolyte in a complex reaction and jointly participated in the generation of CO_2 gas. Also, generated CO_2 gas was observed more early before the voltage plateau. As for the CO_2 outgassing, Renfrew and McCloskey[92] pointed out that the existence of residual lithium carbonate (Li_2CO_3) on the surface of $Li_{1.2}Ni_{0.15}Co_{0.1}Mn_{0.55}O_2$ had a direct correlation with the amount of CO_2 by combining the in situ mass spectrometry, isotopic labeling, and surface carbonate titration techniques. An interesting fact they found was that majority of CO_2 gas generated in the first charge resulted from residual surface Li_2CO_3 oxidation instead of electrolyte oxidation. In addition, unlike the formation of peroxide-like intermediate species ($O^{2-/(2-n)-}$ redox) reported by other research groups before,[93–95] Bruce’s group established a model to illustrate the formation of electron hole states on oxygen during charging.[91] As shown in Figure 13c, each O ion is surrounded by three Li ions from lithium layer and three other cations from transition metal layer. The localized holes are generated in the coordinated O 2p state surrounded by Mn^{4+} and Li^+, which is less covalent and dominates the whole region of 4.5 V. It has been claimed that Mn plays a special role in promoting the localization of electron holes on

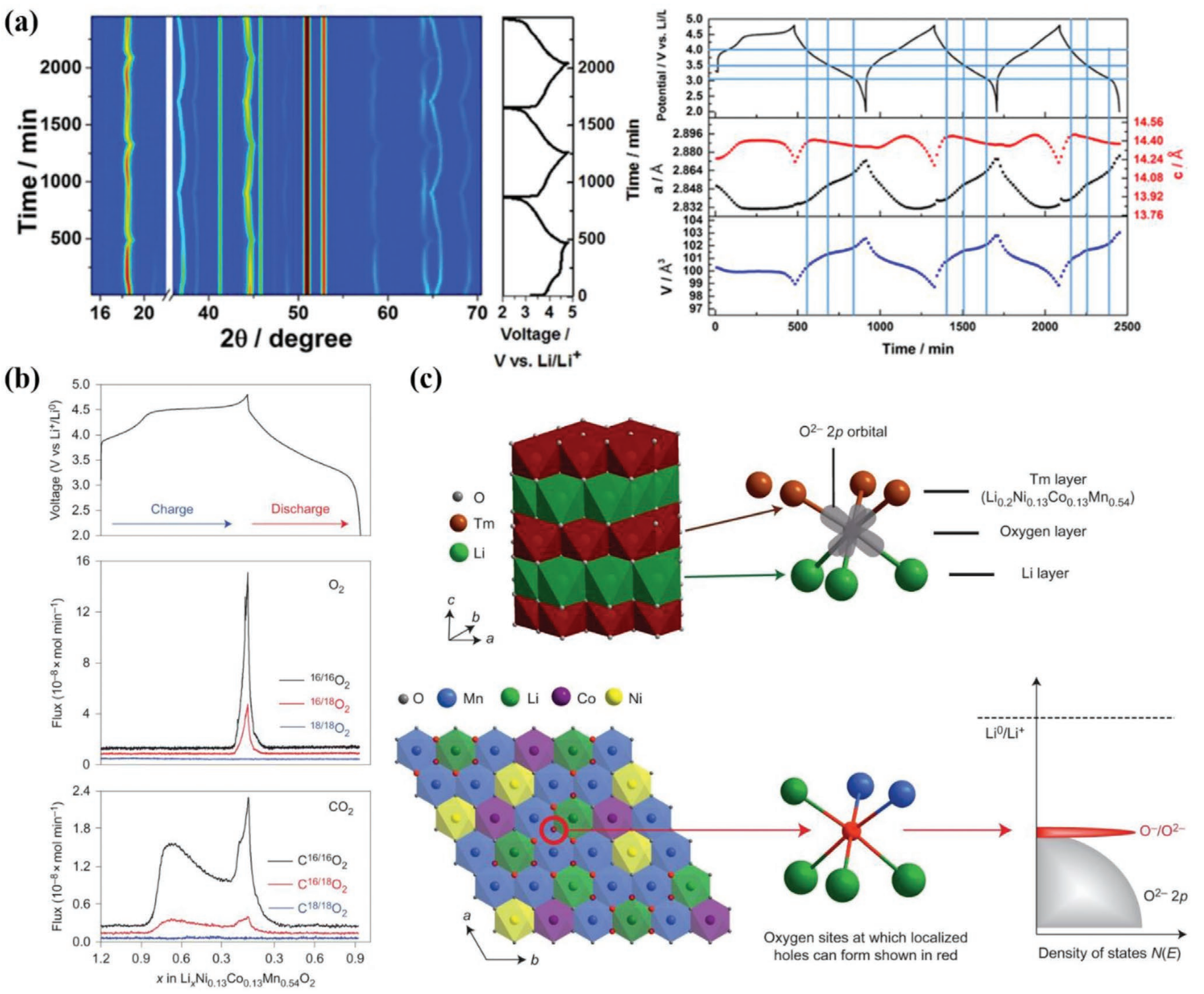

Figure 13. a) Contour maps and change in cell parameters during initial three cycles. Reproduced with permission.[77] Copyright 2018, American Chemical Society. b) DEMS results of the ^{18}O-labeled $Li_{1.2}Ni_{0.13}Co_{0.13}Mn_{0.54}O_2$ in the first cycle. c) Schematic diagram of the location of oxygen anions in Li-rich Mn-based cathode materials at which localized electron–hole states form. Reproduced with permission.[91] Copyright 2016, Nature Publishing Group.

O, which determines the delicate balance between oxygen loss and oxygen redox. Recently, many efforts have been devoted to illuminating whether irreversible oxygen loss occurs on the surface or bulk phase of Li-rich Mn-based cathode materials.[82,96,97] Koga et al.[11,82] proposed a complicated mechanism to explain the anionic redox, which was the reversible oxidation of oxygen in the bulk phase of the particles coupled with irreversible oxygen loss that occurred on the surface. Neutron diffraction, HAADF-STEM, and Raman spectroscopy were utilized to prove that O_2 gas was evolved from the surface and transition metal ions migrated from the surface to the bulk without causing serious structural changes.

Another key issue is that oxygen release from oxide-based cathode materials will leave oxygen vacancies in the bulk or on the surface. Regarding the formation of oxygen vacancies in Li-rich Mn-based cathode materials, there are two sources that need to be clarified. On the one hand, intrinsic oxygen vacancies are commonly formed under the heat treatment conditions during the synthesis of the preliminary compound. This situation is usually due to the escape of oxygen atoms from the lattice under high temperature. For example, Nakamura et al.[98] studied oxygen deficient nonstoichiometry $Li_{1.2}Mn_{0.6}Ni_{0.2}O_{2-\delta}$ through the defect chemistry and thermodynamic analysis. It was observed that the formation of intrinsic oxygen vacancies provoked the reduction expansion of the lattice. Recently, Ma et al.[99] utilized the template-free method to synthesize unique double-shell Li-rich Mn-based cathode material hollow microspheres. The intrinsic oxygen vacancies confirmed by XPS spectra were able to accelerate the kinetic process of lithium ions, which was favorable to enhance the structural stability. On the other hand, it happens at the electrochemical activation stage of the Li_2MnO_3 component under high potential. In this case, Li^+ and O^{2-} are extracted from composite structure in the form of Li_2O, resulting in oxygen vacancies. Qiu et al.[46] adopted a gas-solid interface modification strategy to uniformly introduce oxygen vacancies on the surface of pristine Li-rich Mn-based cathode materials without affecting the structural integrity, and confirmed the amount of oxygen vacancies by neutron diffraction (ND). Calculation results based on first principles showed that oxygen vacancies could effectively reduce the migration energy barrier and promote diffusion process. Moreover, operando differential electrochemical mass spectrometry (DEMS) results revealed that the introduction of oxygen vacancies could suppress the subsequent oxygen release and generate less O_2 gas. Aside from generating oxygen vacancies, oxygen release will weaken the bond between transition metals and oxygen, making it easier for the transition metal to migrate into the lithium site and triggering phase transformation. By combining soft X-ray absorption spectroscopy (XAS), electron energy loss spectroscopy (EELS) and in situ XRD techniques, Hu et al.[48] explained the complexity between oxygen release and structural stability, and demonstrated that AlF_3 coating could greatly inhibit structural degradation by reducing oxygen release. Actually, surface modification is a commonly used strategy to improve the interface properties and control the oxygen activation center for the purpose of a stable structure.

Therefore, how do anionic redox activities play a role in the first cycle of Li-rich Mn-based cathode materials? According to the previous researches, combined with in situ surface enhanced Raman spectroscopy (SERS) to study the surface reaction between Li-rich cathode and graphite anode, Hy et al.[100] gave a comprehensive reaction mechanism of the oxygen-activated components during the charging and discharging process (**Figure 14**). At the start of the first cycle, charge compensation is mainly finished by $Ni^{2+/4+}$ and $Co^{3+/4+}$ redox couples. In this slope stage, a layer of solid electrolyte interface (SEI) film is formed on the anode side and a certain amount of Li_2CO_3 is distributed on the cathode side due to interaction with the electrolyte. As it reaches the plateau period, the activation of Li_2MnO_3 phase will cause the removal of oxygen and lithium ions in the form of Li_2O. Simultaneously, partial oxygen anions begin to contribute to the specific capacity in the reversible redox of $O^{2-/-}$. Under such a high charging potential, the ester electrolyte is likely to be oxidized and decomposed into gases such as CO and CO_2. At the end of the first charge, the unstable layered structure not only easily initiates the release of O_2, but also reacts with the electrolyte to form protons (H^+) through a catalytic-like reaction at the interface. Several studies have pointed out that protons (H^+) can exchange with lithium ions one to one in electrochemical activities.[101–104] For example, Robertson et al.[102] reported that the H^+ ions generated by the oxidation of nonaqueous electrolyte would replace the lithium ions in the Li_2MnO_3 system. In the following discharge process, the discharge compensation mechanism is usually considered to be the joint participation of $Ni^{4+/2+}$ redox couples, $Mn^{4+/3+}$ redox couples and $O^{-/2-}$ redox couples, which increases continuously with the cycle number. It is noteworthy that the appearance of trivalent manganese ions (Mn^{3+}) is the root cause of Jahn–Teller distortion effect, which affects molecular symmetry.[105,106] In the final stage of the discharge process, the formation of LiOH on the anode and Li_2CO_3 on the cathode results in the solution to change from an acidic environment to a more neutral environment, thereby increasing the electrochemical impedance.

4.3. Anionic/Cationic Redox Interplay

It has been acknowledged that Li-rich Mn-based cathode materials have a special double redox mechanism, including anionic redox and cationic redox. But how they affect and interplay with each other during cycling still remains a difficulty in current

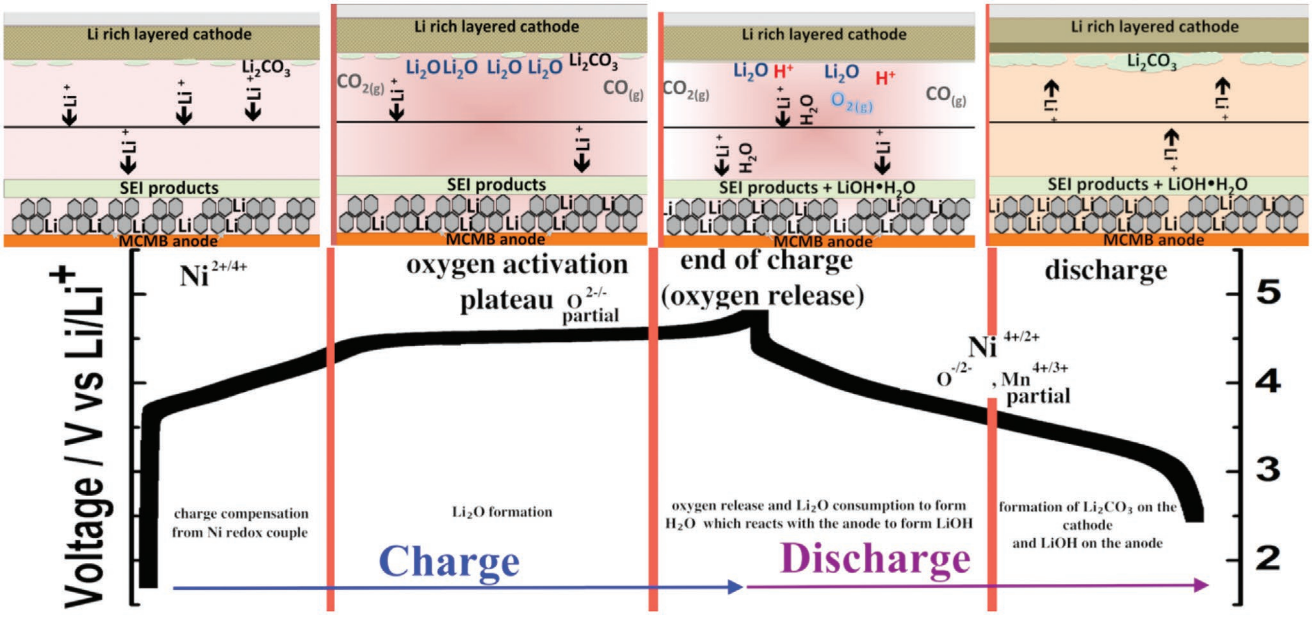

Figure 14. Surface reaction mechanism of Li-rich Mn-based cathode materials during the first charge/discharge process. Reproduced with permission.[100] Copyright 2014, American Chemical Society.

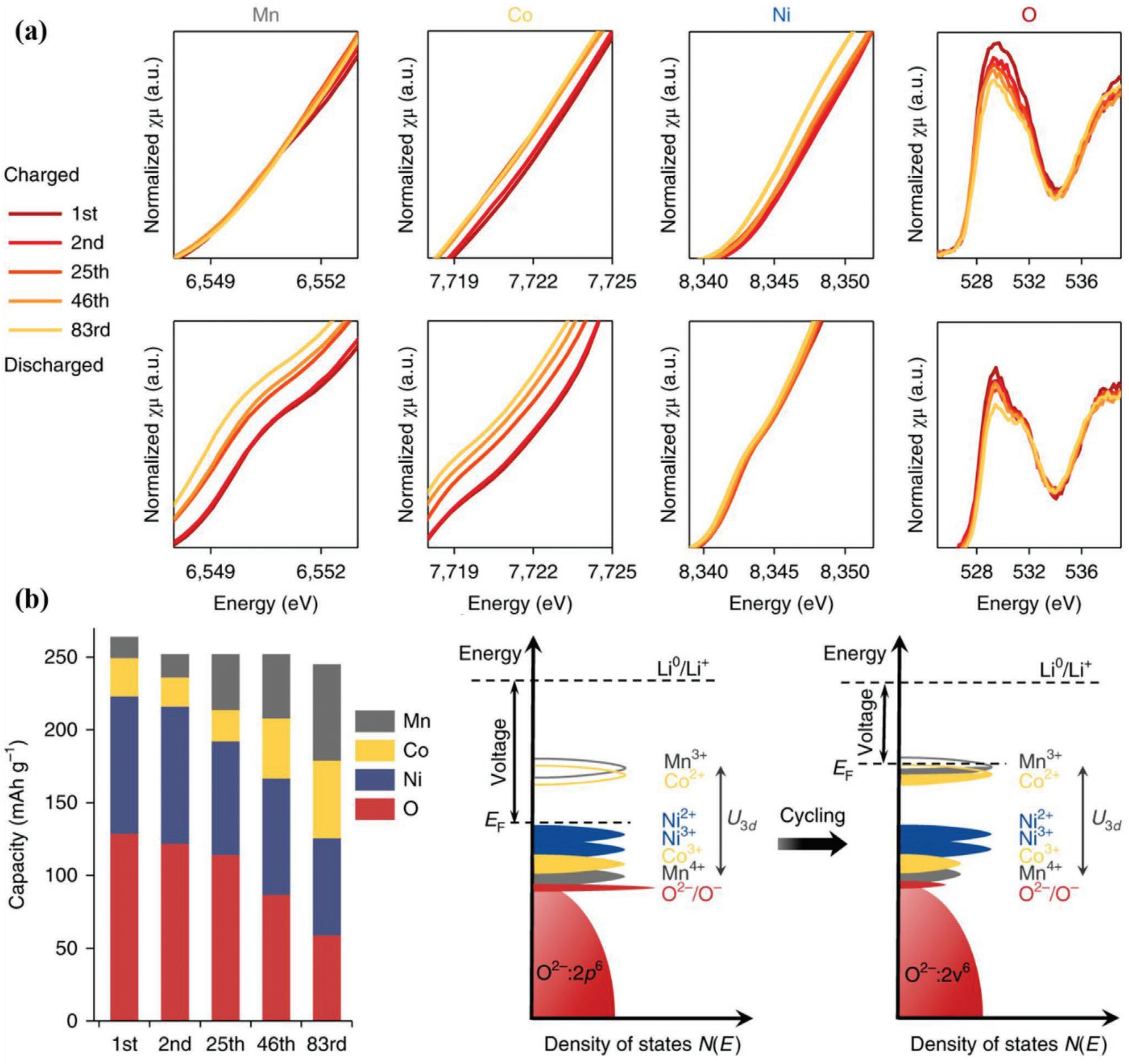

Figure 15. a) K-edge XAS results of Mn, Co, Ni, and O elements of $Li_{1.2}Ni_{0.15}Co_{0.1}Mn_{0.55}O_2$ cathode materials after different cycles. b) The contribution of different elements to the discharge capacity during cycling and illustration of Fermi level rising due to changes in electronic structure. Reproduced with permission.[48] Copyright 2018, Nature Publishing Group.

research. Hu et al.[48] conducted X-ray absorption near-edge structure spectroscopy (XANES) to perform the ex situ test on the K-edge absorption of the Mn, Co, Ni and O elements of $Li_{1.2}Ni_{0.15}Co_{0.1}Mn_{0.55}O_2$ cathode materials in different cycles (the 1st, 2nd, 25th, 46th, and 83rd cycles). As shown in **Figure 15**a, a unique discovery is that the average valence state of all transition metal cations obtained by X-ray absorption spectroscopy gradually decreases with the increase of cycle number. In addition, based on the semiquantitative analysis of the XAS results, it can be found that the contribution of the oxygen ion redox couple (O^{2-}/O^-) and nickel ion redox couple ($Ni^{2+}/Ni^{3+}/Ni^{4+}$) to the overall discharge capacity gradually decreases with the progress of cycling. On the contrary, the contribution of the cobalt ion redox couple (Co^{2+}/Co^{3+}) and manganese ion redox couple (Mn^{3+}/Mn^{4+}) to the overall discharge capacity gradually increases with the progress of cycling. It is not difficult to see that cobalt ions and manganese ions are playing an increasingly important role in compensating for capacity decay in long cycling (Figure 15b). This shifting of redox couples from nickel/oxygen to manganese/cobalt is also an important cause of voltage decay. In the energy band structure of the insertion/extraction layered oxides, the redox potential is closely related to the Fermi level. The holes above the Fermi level and the electrons below the Fermi level form a redox couple, and the open-circuit voltage (OCV) of the battery is usually determined by the relative Fermi level energy.[107] This enables to transfer electrons from the cathode side to the anode side. The Fermi level is mainly above the Ni^{2+}/Ni^{3+} redox couple in the pristine sample. After starting the electrochemical activity, the occurrence of oxygen loss leads to the reduction of transition metals. Especially for the nickel element, it is likely to participate in the formation of a surface reduced layer, and even result in a layered to spinel phase transformation.[108] While for manganese and cobalt elements, the activation of Mn^{3+}/Mn^{4+} and Co^{2+}/Co^{3+} redox couples raises the Fermi level and leads to a decrease in open-circuit voltage and operating voltage. Furthermore, the reduction of transition metal elements also weakens the covalency between transition metals and oxygen, accounting for less oxygen participating in the redox. Additional evidence is that Assat et al.[109] observed that oxygen redox contribution had decreased with the increased contribution of Mn redox in $Li_{1.2}Ni_{0.13}Mn_{0.54}Co_{0.13}O_2$ materials over long cycling via hard X-ray photoemission spectroscopy (HAXPES).

4.4. O_2-Type Li-Rich Mn-Based Structure

Compared with traditional O_3-type Li-rich Mn-based cathode materials, O_2-type cathode materials can inhibit the formation of oxygen-oxygen dimers and irreversible phase transformations during cycling. It is well known that Li-rich Mn-based cathode materials used in large amounts of synthesis and research previously are mainly O_3-type structures characterized by oxygen stacking in ABCABC mode. This structure can provide a discharge capacity of up to 250–300 mAh g^{-1}. However, the oxygen redox reaction caused by the activation of the Li_2MnO_3 components inherent in this structure promotes the migration of transition metal ions, leading to the transformation from layered to spinel phases, severe voltage and capacity fading during cycling, which is the main obstacle hindering commercial application. As early as 1999, Paulsen et al.[110] reported a new type of layered Li-Mn oxide with the O_2 structure of ABCBA oxygen packing which did not convert to spinel, but the specific capacity was only 150 mAh g^{-1}. In 2018, Zuo et al.[111] synthesized the O_2-type Li-rich Mn-based cathode materials by molten salt exchange method. The XRD patterns showed that the prepared $Li_{1.25}Co_{0.25}Mn_{0.50}O_2$ material was mainly an O_2-type layered oxide with a single-layer Li_2MnO_3 superstructure (**Figure 16**a), and its crystal structure model was shown in Figure 16b. This structure not only achieved a reversible discharge specific capacity of up to 400 mAh g^{-1} in the first cycle, but also obtained a high initial Coulombic efficiency of 99.5%, which could provide higher energy density (Figure 16c). The high initial Coulombic efficiency indicated that oxygen anions contributed to the overall specific capacity in the form of reversible anionic redox instead of irreversible oxygen loss, and the local oxygen structure remained stable. After 50 cycles, the average voltage decay was only 0.07 V (Figure 16d). These excellent electrochemical properties also demonstrated that the O_2-type structure possessed strong structural stability and could effectively suppress irreversible phase transformation. Eum et al.[112] proved that the reversibility

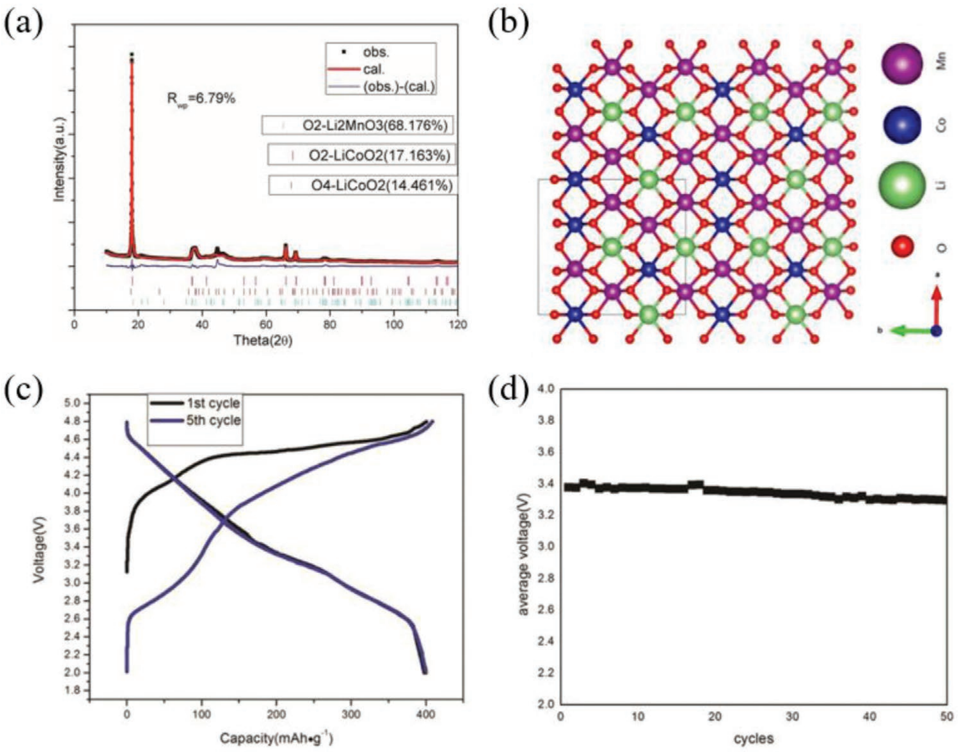

Figure 16. a) Rietveld refinement of XRD patterns of O_2-type Li-rich Mn-based cathode materials. b) Crystal structure model of O_2-type Li-rich Mn-based cathode materials. c) Charge–discharge curves of O_2-type Li-rich Mn-based cathode materials. d) Discharge average voltage of O_2-type Li-rich Mn-based cathode materials. Reproduced with permission.[111] Copyright 2018, Wiley-VCH.

of transition metal cation migration could be dramatically improved by adjusting oxygen packing patterns in the Li-rich Mn-based cathode materials. The enhanced reversibility in the O_2-type structure could reduce the asymmetry of anionic redox in traditional O_3-type structure and promote the reduction of high potential anions, thereby suppressing the subsequent voltage decay. Most recently, Cui et al.[113] utilized a highly stable O_2-type $Li_{1.2}Ni_{0.13}Mn_{0.54}Co_{0.13}O_2$ cathode material and all-fluorinated electrolyte to improve the interfacial stability and suppress the irreversible oxygen release. The cathode material with the O_2-type structure could prevent transition metal ions from migrating to the lithium layer, and form a stable fluorine-containing SEI film at the interface between cathode and electrolyte, thereby inhibiting the structural transformation and oxygen release. As a result, the O_2-type $Li_{1.2}Ni_{0.13}Mn_{0.54}Co_{0.13}O_2$ material in all-fluorinated electrolyte delivered a reversible discharge specific capacity of 278.3 mAh g^{-1} with a superior initial Coulombic efficiency of 99.82%. And an excellent capacity retention of 83.3% after 100 cycles was also obtained. The O_2-type layered oxides provide new ideas for improving Li-rich Mn-based cathode materials and designing higher energy storage materials.

Anionic redox activities are usually closely related to high capacity of Li-rich Mn-based cathode materials. It should be noted that the anionic redox process involves a multielectron process to provide higher capacity, which threatens the structural stability of the cathode material and seriously affect its cycle life. Therefore, for the high-capacity Li-rich Mn-based cathode material based on anionic redox, both the reversibility of anion redox and the stability of the host structure should be considered. Anionic redox can be tuned toward a favorable process by adjusting the electronic structure of the covalent bond between the transition metal and oxygen. Essentially, the typical feature of Li-rich Mn-based cathode materials is that the content of lithium ions is more than that of transition metal ions, which ultimately triggers anion redox. An extreme case is the electrode reaction will be similar to that in a lithium–oxygen battery when lithium ions completely replace other metal ions. Therefore, one of the valuable directions is to promote more anions to participate in reversible electrode reaction. However, the key problem is how to reach a compromise between structural stability and capacity. In addition, the irreversible oxygen loss can also be suppressed by changing the oxygen stacking mode in the layered structure, so that the anionic redox progresses toward a more reversible form.

Importantly, it must be noted that there are inextricable intrinsic relations among atoms, lattices, and dimensions, though the above sections are presented as different levels from top to bottom. The reversibility of anionic redox is highly dependent on the surrounding chemical environment such as atom stacking mode, and bond interplay with cations, which also directly affects ordering/disordering arrangement of atoms. Furthermore, the interlayer or intralayer movement of transition metal ions inevitably causes the change of its fine layered lattice structure. The phase composition and transformation in the synthesis process are delicately regulated by the arrangement and embedding of atoms, and are extremely susceptible to the influence of atomic activities. The nucleation and growth process of the crystal ultimately determines the macroscopic morphology and size of cathode materials, and accounts for the difference in their overall performance. Besides, electrode fabrication is also in the same boat as all the issue, since the surface and interface of the cathode materials play an important role in improving electrochemical performance. Undoubtedly, a slight move in any part may affect the situation as a whole. It is necessary for developing the Li-rich Mn-based cathode materials to both understand deeply mechanism of every key step and coordinate systematically the whole.

5. Conclusions and Future Perspectives

Li-rich Mn-based cathode materials are being understood more in-depth with the development of state-of-the-art characterization technology. The perspective from dimension to lattice to atom reveals the subtle and critical changes in the different levels during charge and discharge process of the promising cathode material. The regulation of dimensionality can serve as a connecting link between the macroscopical and microcosmic issues, which can be conducive to not only accelerating kinetics of the electrode processes, but also improving the overall tap density for realizing high energy density, structural stability and thermal stability for long cycling. Furthermore, the structural degradation of Li-rich Mn-based cathode materials during cycling is closely related to the irreversible phase transformation, which also accounts for the severe voltage and capacity decay. The migration of transition metal ions into the lithium layer is the main driving force for this irreversible phase transformation process. How to design effective strategies to suppress the transformation from layered to spinel phase or even rock salt phase during cycling has always been the key issue to Li-rich Mn-based cathode materials. Besides, it has been acknowledged that unstable anionic redox activity plays an important role in the structural transformation from surface to the bulk phase. In particular, the oxygen loss induced by the oxidation of the lattice oxygen will generate oxygen vacancies on the surface of the cathode material, thereby triggering continuous microstructural changes. How to inhibit irreversible oxygen loss is an important way to enhance structural stability of Li-rich Mn-based cathode materials. The recent findings enable us to have a new and comprehensive understanding toward the effect of lithium and oxygen on the phase transformation during the insertion/extraction process.

In the future researches, the inmost mechanism on evolution of Li-rich Mn-based cathode materials during the whole life cycle is still the crucial issue for addressing the challenges, and a systematical research from the atomic and ionic level (bottom) to the final performance in a practical battery (top) is undoubtedly more credible than the partial studies easily producing contradictory understandings. Though it is not easy to verify an entirely self-consistent mechanism from bottom to top, the combination of advanced characterization techniques with higher test accuracy and real-time observation at a more microscopic level make it worth pursuing. Especially, the development of various advanced in situ characterization techniques, including in situ X-ray technology, in situ optical technology and in situ electronic imaging technology, provides an important basis for in-depth study of the microscopic mechanism.

Moreover, a lot of activities of the cathode material are often closely related to the interfacial composition and stability. The research on the ion and electron transport process at the interface may have a profound impact on improving the structural stability and electrochemical performance of Li-rich Mn-based cathode materials. Besides the anionic redox mechanism, new alternative explanations for the origin of the anomalous capacity of Li-rich Mn-based cathode materials are also worth exploring, such as the Mn^{4+}/Mn^{7+} redox[76] mentioned before. It is possible to design a cathode material that utilizes high oxidation states without inducing transition metal migration, or design a material with facile and reversible migration to realize satisfactory electrochemical performance.

From the perspective of composition design, alternative elements should be selected on the basis of chemical compatibility and redox compatibility. Transition metal elements with redox activity should be preferentially selected to obtain larger capacity, such as V^{3+} and Cr^{3+} with multielectron redox capability. For high-valent metals with nonredox activity, such as Ti^{4+} and Nb^{5+}, they can be used as the source of charge compensator. The cathode materials composed of a large number of metal ion species should be paid more attention, because the superior compositional flexibility provides more possibilities for designing high-entropy materials. Li-rich Mn-based cathode materials can appropriately incorporate a large number of transition metal species to enhance the flexibility of its chemical composition. In addition, cobalt-free Li-rich Mn-based cathode materials will get more attention due to the high cost and high toxicity of cobalt. To match and screen an ideal composition, theoretical simulation based on big data and machine learning will become a powerful tool for revealing complex rule patterns and constructing chemical composition. This will not only help guide the synthesis of new energy storage materials, but also promote the pace of research and development technology informatization.

At present, the research of cathode materials based on surface coating, element doping and structural design has made important progress in various aspects. However, it can be noted that a single strategy usually only solves specific problems and achieve finite improvements, which is difficult to satisfy multiple requirements. For the practical application, the environment and the challenges that the cathode material faces are often multifaceted. Therefore, the comprehensive application and integration strategies of multiple modification methods should be developed in order to solve the various problems and promote overall performance of Li-rich Mn-based cathode materials.

Throughout the development history of lithium-ion batteries, most of cathode materials have experienced a time span of decades from discovery, research to final industrialization. After Li-rich Mn-based cathode materials have been studied intensively for more than ten years, more and more deep insights into the promising materials are being gained. We have reason to believe that the current challenges can be solved in the near future.

Acknowledgements

This work was supported by the National Key Research and Development Program (2016YFB0100200). The authors greatly thank the financial fund from Natural Science Foundation of Tianjin (18JCZDJC31000).

Conflict of Interest

The authors declare no conflict of interest.

Keywords

anionic redox, Li-rich cathode materials, microscopic dimension, phase transformation

Received: December 16, 2020
Revised: February 25, 2021

---

[1] M. Rossouw, M. Thackeray, *Mater. Res. Bull.* **1991**, *26*, 463.
[2] J. M. Tarascon, M. Armand, *Nature* **2001**, *414*, 359.
[3] a) G. Assat, J. M. Tarascon, *Nat. Energy* **2018**, *3*, 373; b) P. Y. Hou, H. Z. Zhang, Z. Y. Zi, L. Q. Zhang, X. J. Xu, *J. Mater. Chem. A* **2017**, *5*, 4254; c) G. Liu, S. Li, J. Mei, L. M. Liu, Y. Cui, H. Liu, *J. Power Sources* **2017**, *353*, 51.
[4] J. Rana, M. Stan, R. Kloepsch, J. Li, G. Schumacher, E. Welter, I. Zizak, J. Banhart, M. Winter, *Adv. Energy Mater.* **2014**, *4*, 1300998.
[5] N. Yabuuchi, M. Takeuchi, M. Nakayama, H. Shiiba, M. Ogawa, K. Nakayama, T. Ohta, D. Endo, T. Ozaki, T. Inamasu, K. Sato, S. Komaba, *Proc. Natl. Acad. Sci. USA* **2015**, *112*, 7650.
[6] B. Li, H. J. Yan, J. Ma, P. R. Yu, D. G. Xia, W. F. Huang, W. S. Chu, Z. Y. Wu, *Adv. Funct. Mater.* **2014**, *24*, 5112.
[7] S. L. Cui, X. Zhang, X. W. Wu, S. Liu, G. R. Li, X. P. Gao, *ACS Appl. Mater. Interfaces* **2020**, *12*, 47655.
[8] a) Y. Y. Liu, Z. Yang, J. L. Li, B. B. Niu, K. Yang, F. Y. Kang, *J. Mater. Chem. A* **2018**, *6*, 13883; b) F. H. Ning, B. Li, J. Song, Y. X. Zuo, H. F. Shang, Z. M. Zhao, Z. Yu, W. S. Chu, K. Zhang, G. Feng, X. Y. Wang, D. G. Xia, *Nat. Commun.* **2020**, *11*, 4973; c) W. Liu, J. X. Li, W. T. Li, H. Y. Xu, C. Zhang, X. P. Qiu, *Nat. Commun.* **2020**, *11*, 3629; d) Y. Zheng, L. Chen, Y. F. Su, J. Tan, L. Y. Bao, Y. Lu, J. Wang, R. J. Chen, S. Chen, F. Wu, *J. Mater. Chem. A* **2017**, *5*, 24292; e) M. Han, J. Y. Jiao, Z. P. Liu, X. Shen, Q. H. Zhang, H. J. Lin, C. T. Chen, Q. Y. Kong, W. K. Pang, Z. P. Guo, R. C. Yu, L. Gu, Z. W. Hu, Z. X. Wang, L. Q. Chen, *Adv. Energy Mater.* **2020**, *10*, 1903634.
[9] S. L. Cui, Y. Y. Wang, S. Liu, G. R. Li, X. P. Gao, *Electrochim. Acta* **2019**, *328*, 135109.
[10] K. Ku, J. Hong, H. Kim, H. Park, W. M. Seong, S. K. Jung, G. Yoon, K. Y. Park, H. Kim, K. Kang, *Adv. Energy Mater.* **2018**, *8*, 1800606.
[11] H. Koga, L. Croguennec, M. Ménétrier, P. Mannessiez, F. Weill, C. Delmas, *J. Power Sources* **2013**, *236*, 250.
[12] B. Xu, C. R. Fell, M. Chi, Y. S. Meng, *Energy Environ. Sci.* **2011**, *4*, 2223.
[13] D. Y. W. Yu, K. Yanagida, *J. Electrochem. Soc.* **2011**, *158*, A1015.
[14] Z. Q. Deng, A. Manthiram, *J. Phys. Chem. C* **2011**, *115*, 7097.
[15] a) Y. J. Lee, M. G. Kim, J. Cho, *Nano Lett.* **2008**, *8*, 957; b) V. Hebbar, M. Viji, A. K. Budumuru, S. Gautam, K. H. Chae, K. Balaji, N. T. Kalyana Sundaram, A. K. Subramani, C. Sudakar, *ACS Appl. Mater. Interfaces* **2020**, *12*, 32566; c) J. X. Liu, J. Q. Wang, Y. X. Ni, Y. D. Zhang, J. Luo, F. Y. Cheng, J. Chen, *Small Methods* **2019**, *3*, 1900350; d) G. Ma, S. Li, W. X. Zhang, Z. H. Yang, S. L. Liu, X. M. Fan, F. Chen, Y. Tian, W. B. Zhang, S. H. Yang, M. Li, *Angew. Chem., Int. Ed.* **2016**, *55*, 3667.
[16] a) G. Z. Wei, X. Lu, F. S. Ke, L. Huang, J. T. Li, Z. X. Wang, Z. Y. Zhou, S. G. Sun, *Adv. Mater.* **2010**, *22*, 4364; b) D. Wang, I. Belharouak, G. Zhou, K. Amine, *Adv. Funct. Mater.* **2013**, *23*, 1070.
[17] a) H. J. Kim, H. G. Jung, B. Scrosati, Y. K. Sun, *J. Power Sources* **2012**, *203*, 115; b) X. Li, Z. Cao, H. Yue, Q. Wang, H. Zhang, S. T. Yang, *ACS Sustainable Chem. Eng.* **2019**, *7*, 5946.

[18] a) L. J. Zhang, N. Li, B. R. Wu, H. L. Xu, L. Wang, X. Q. Yang, F. Wu, *Nano Lett.* **2015**, *15*, 656; b) P. Oh, S. Myeong, W. Cho, M. J. Lee, M. Ko, H. Y. Jeong, J. Cho, *Nano Lett.* **2014**, *14*, 5965; c) M. Xu, L. Fei, W. Zhang, T. Li, W. Lu, N. Zhang, Y. Lai, Z. Zhang, J. Fang, K. Zhang, J. Li, H. Huang, *Nano Lett.* **2017**, *17*, 1670.

[19] F. Fu, Y. Yao, H. Wang, G. L. Xu, K. Amine, S. G. Sun, M. Shao, *Nano Energy* **2017**, *35*, 370.

[20] a) Y. K. Sun, S. T. Myung, M. H. Kim, J. Prakash, K. Amine, *J. Am. Chem. Soc.* **2005**, *127*, 13411; b) Y. K. Sun, S. T. Myung, B. C. Park, J. Prakash, I. Belharouak, K. Amine, *Nat. Mater.* **2009**, *8*, 320; c) Y. K. Sun, Z. Chen, H. J. Noh, D. J. Lee, H. G. Jung, Y. Ren, S. Wang, C. S. Yoon, S. T. Myung, K. Amine, *Nat. Mater.* **2012**, *11*, 942.

[21] J. Li, J. Camardese, R. Shunmugasundaram, S. Glazier, Z. Lu, J. R. Dahn, *Chem. Mater.* **2015**, *27*, 3366.

[22] T. H. Wu, X. Liu, X. Zhang, Y. Lu, B. Wang, Q. S. Deng, Y. B. Yang, E. Wang, Z. T. Lyu, Y. Q. Li, Y. T. Wang, Y. Lyu, C. F. He, Y. Ren, G. L. Xu, X. L. Sun, K. Amine, H. J. Yu, *Adv. Mater.* **2020**, *7*, 2001358.

[23] a) J. Gao, A. Manthiram, *J. Power Sources* **2009**, *191*, 644; b) E. S. Lee, A. Manthiram, *J. Electrochem. Soc.* **2011**, *158*, A47.

[24] F. Wu, Z. Wang, Y. Su, N. Yan, L. Bao, S. Chen, *J. Power Sources* **2014**, *247*, 20.

[25] A. Manthiram, J. C. Knight, S. T. Myung, S. M. Oh, Y. K. Sun, *Adv. Energy Mater.* **2016**, *6*, 1501010.

[26] J. Q. Zhao, R. M. Huang, W. P. Gao, J. M. Zuo, X. F. Zhang, S. T. Misture, Y. Chen, J. V. Lockard, B. L. Zhang, S. M. Guo, M. R. Khoshi, K. Dooley, H. X. He, Y. Wang, *Adv. Energy Mater.* **2015**, *5*, 1401937.

[27] M. M. Thackeray, C. S. Johnson, J. T. Vaughey, N. Li, S. A. Hackney, *J. Mater. Chem.* **2005**, *15*, 2257.

[28] W. D. Li, H. Y. Asl, Q. Xie, A. Manthiram, *J. Am. Chem. Soc.* **2019**, *141*, 5097.

[29] A. O. Kondrakov, A. Schmidt, J. Xu, H. Geßwein, R. Mönig, P. Hartmann, H. Sommer, T. Brezesinski, J. Janek, *J. Phys. Chem. C* **2017**, *121*, 3286.

[30] H.-H. Sun, A. Manthiram, *Chem. Mater.* **2017**, *29*, 8486.

[31] J. Li, R. Shunmugasundaram, R. Doig, J. R. Dahn, *Chem. Mater.* **2016**, *28*, 162.

[32] C. H. Shen, S. Y. Shen, F. Fu, C. G. Shi, H. Y. Zhang, M. J. Pierre, H. Su, Q. Wang, B. B. Xu, L. Huang, J. T. Li, S. G. Sun, *J. Mater. Chem.* **2015**, *3*, 12220.

[33] K. Shimoda, M. Oishi, T. Matsunaga, M. Murakami, K. Yamanaka, H. Arai, Y. Ukyou, Y. Uchimoto, T. Ohta, E. Matsubara, Z. Ogumi, *J. Mater. Chem.* **2017**, *5*, 6695.

[34] F. Zheng, C. Yang, X. Xiong, J. Xiong, R. Hu, Y. Chen, M. Liu, *Angew. Chem., Int. Ed.* **2015**, *54*, 13058.

[35] S. H. Lee, J. S. Moon, M. S. Lee, T. H. Yu, H. Kim, B. M. Park, *J. Power Sources* **2015**, *281*, 77.

[36] J. R. Croy, M. Balasubramanian, K. G. Gallagher, A. K. Burrell, *Acc. Chem. Res.* **2015**, *48*, 2813.

[37] Z. Lu, L. Y. Beaulieu, R. A. Donaberger, C. L. Thomas, J. R. Dahn, *J. Electrochem. Soc.* **2002**, *149*, A778.

[38] M. Gu, I. Belharouak, A. Genc, Z. G. Wang, D. P. Wang, K. Amine, F. Gao, G. W. Zhou, S. Thevuthasan, D. R. Baer, J. G. Zhang, N. D. Browning, J. Liu, C. M. Wang, *Nano Lett.* **2012**, *12*, 5186.

[39] H. Yu, H. Kim, Y. Wang, P. He, D. Asakura, Y. Nakamura, H. Zhou, *Phys. Chem. Chem. Phys.* **2012**, *14*, 6584.

[40] B. Song, M. O. Lai, L. Lu, *Electrochim. Acta* **2012**, *80*, 187.

[41] D. Luo, G. S. Li, C. C. Fu, J. Zheng, J. M. Fan, Q. Li, L. P. Li, *Adv. Energy Mater.* **2014**, *4*, 1400062.

[42] S. L. Pang, M. Zhu, K. J. Xu, X. Q. Shen, H. R. Wen, Y. J. Su, G. M. Yang, X. Wu, S. W. Li, W. Z. Wang, X. M. Xi, H. B. Wang, *J. Electrochem. Soc.* **2018**, *165*, A1897.

[43] R. P. Qing, J. L. Shi, D. D. Xiao, X. D. Zhang, Y. X. Yin, Y. B. Zhai, L. Gu, Y. G. Guo, *Adv. Energy Mater.* **2016**, *6*, 1501914.

[44] C. Storey, I. Kargina, Y. Grincourt, I. J. Davidson, Y. C. Yoo, D. Y. Seung, *J. Power Sources* **2001**, *97–98*, 541.

[45] K. A. Jarvis, Z. Q. Deng, L. F. Allard, A. Manthiram, P. J. Ferreira, *Chem. Mater.* **2011**, *23*, 3614.

[46] B. Qiu, M. H. Zhang, L. J. Wu, J. Wang, Y. G. Xia, D. N. Qian, H. D. Liu, S. Hy, Y. Chen, K. An, Y. M. Zhu, Z. P. Liu, Y. S. Meng, *Nat. Commun.* **2016**, *7*, 12108.

[47] H. J. Yu, R. Ishikawa, Y. G. So, N. Shibata, T. Kudo, H. S. Zhou, Y. Ikuhara, *Angew. Chem., Int. Ed.* **2013**, *52*, 5969.

[48] E. Y. Hu, X. Q. Yu, R. Q. Lin, X. X. Bi, J. Lu, S. Bak, K. W. Nam, H. L. Xin, C. Jaye, D. A. Fischer, K. Amine, X. Q. Yang, *Nat. Energy* **2018**, *3*, 690.

[49] N. Tran, L. Croguennec, M. Ménétrier, F. Weill, Ph. Biensan, C. Jordy, C. Delmas, *Chem. Mater.* **2008**, *20*, 4815.

[50] Q. Q. Li, Z. P. Yao, E. Lee, Y. B. Xu, M. M. Thackeray, C. Wolverton, V. P. Dravid, J. S. Wu, *Nat. Commun.* **2019**, *10*, 1692.

[51] P. F. Yan, J. M. Zheng, Z. K. Tang, A. Devaraj, G. Y. Chen, K. Amine, J. G. Zhang, L. M. Liu, C. M. Wang, *Nat. Nanotechnol.* **2019**, *14*, 602.

[52] Y. X. Tang, Y. Y. Zhang, W. L. Li, B. Ma, X. D. Chen, *Chem. Soc. Rev.* **2015**, *44*, 5926.

[53] a) A. Boulineau, L. Simonin, J. F. Colin, C. Bourbon, S. Patoux, *Nano Lett.* **2013**, *13*, 3857; b) K. Kleiner, B. Strehle, A. R. Baker, S. J. Day, C. C. Tang, I. Buchberger, F. F. Chesneau, H. A. Gasteiger, M. Piana, *Chem. Mater.* **2018**, *30*, 3656.

[54] L. Gu, D. Xiao, Y. S. Hu, H. Li, Y. Ikuhara, *Adv. Mater.* **2015**, *27*, 2134.

[55] J. Zheng, M. Gu, A. Genc, J. Xiao, P. Xu, X. Chen, Z. Zhu, W. Zhao, L. Pullan, C. Wang, J. G. Zhang, *Nano Lett.* **2014**, *14*, 2628.

[56] P. Yan, A. Nie, J. Zheng, Y. Zhou, D. Lu, X. Zhang, R. Xu, I. Belharouak, X. Zu, J. Xiao, K. Amine, J. Liu, F. Gao, R. Shahbazian-Yassar, J. G. Zhang, C. M. Wang, *Nano Lett.* **2015**, *15*, 514.

[57] W. B. Hua, M. Z. Chen, B. Schwarz, M. Knapp, M. Bruns, J. Barthel, X. S. Yang, Fl. Sigel, R. Azmi, A. Senyshyn, A. Missiul, L. Simonelli, M. Etter, S. Wang, X. K. Mu, A. Fiedler, J. R. Binder, X. D. Guo, S. L. Chou, B. H. Zhong, S. Indris, H. Ehrenberg, *Adv. Energy Mater.* **2019**, *9*, 1803094.

[58] W. B. Hua, S. Wang, M. Knapp, S. J. Leake, A. Senyshyn, C. Richter, M. Yavuz, J. R. Binder, C. P. Grey, H. Ehrenberg, S. Indris, B. Schwarz, *Nat. Commun.* **2019**, *10*, 5365.

[59] M. Gu, I. Belharouak, J. M. Zheng, H. M. Wu, J. Xiao, A. Genc, K. Amine, S. Thevuthasan, D. R. Baer, J. G. Zhang, N. D. Browning, J. Liu, C. M. Wang, *ACS Nano* **2013**, *7*, 760.

[60] B. Song, Z. Liu, M. O. Lai, L. Lu, *Phys. Chem. Chem. Phys.* **2012**, *14*, 12875.

[61] A. Boulineau, L. Simonin, J.-F. Colin, E. Canévet, L. Daniel, S. Patoux, *Chem. Mater.* **2012**, *24*, 3558.

[62] S. H. Kang, P. Kempgens, S. Greenbaum, A. J. Kropf, K. Amine, M. M. Thackeray, *J. Mater. Chem.* **2007**, *17*, 2069.

[63] S. Hy, W.-N. Su, J.-M. Chen, B.-J. Hwang, *J. Phys. Chem. C* **2012**, *116*, 25242.

[64] F. Yang, Y. Liu, S. K. Martha, Z. Wu, J. C. Andrews, G. E. Ice, P. Pianetta, J. Nanda, *Nano Lett.* **2014**, *14*, 4334.

[65] a) B. Li, Y. Yu, J. Zhao, *J. Power Sources* **2015**, *275*, 64; b) S. H. Lee, B. K. Koo, J.-C. Kim, K. M. Kim, *J. Power Sources* **2008**, *184*, 276.

[66] a) Q. Y. Wang, J. Liu, A. V. Murugan, A. Manthiram, *J. Mater. Chem.* **2009**, *19*, 4965; b) R. A. House, G. J. Rees, M. A. Perez-Osorio, J. J. Marie, E. Boivin, A. W. Robertson, A. Nag, M. Garcia-Fernandez, K. J. Zhou, P. G. Bruce, *Nat. Energy* **2020**, *5*, 777; c) Z. Xu, L. J. Ci, Y. F. Yuan, X. K. Nie, J. W. Li, J. Cheng, Q. Sun, Y. M. Zhang, G. F. Han, G. H. Min, J. Lu, *Nano Energy* **2020**, *75*, 104912.

[67] Q. Y. Li, D. Zhou, L. J. Zhang, D. Ning, Z. H. Chen, Z. J. Xu, R. Gao, X. Z. Liu, D. H. Xie, G. Schumacher, X. F. Liu, *Adv. Funct. Mater.* **2019**, *29*, 1806706.

[68] B. Wu, X. K. Yang, X. Jiang, Y. Zhang, H. B. Shu, P. Gao, L. Liu, X. Y. Wang, *Adv. Funct. Mater.* **2018**, *28*, 1803392.

[69] a) S. Liu, Z. P. Liu, X. Shen, W. H. Li, Y. R. Gao, M. N. Banis, M. S. Li, K. Chen, L. Zhu, R. C. Yu, Z. X. Wang, X. L. Sun, G. Lu, Q. Y. Kong, X. D. Bai, L. Q. Chen, *Adv. Energy Mater.* **2018**, *8*, 1802105; b) Y. Wu, A. Manthiram, *Solid State Ion* **2009**, *180*, 50; c) X. Ding, Y. Li, F. Chen, X. D. He, A. Yasmin, Q. Hu, Z. Wen, C. Chen, *J. Mater. Chem. A* **2019**, *7*, 11513.

[70] N. Yabuuchi, K. Yoshii, S. T. Myung, I. Nakai, S. Komaba, *J. Am. Chem. Soc.* **2011**, *133*, 4404.

[71] M. Sathiya, G. Rousse, K. Ramesha, C. P. Laisa, H. Vezin, M. T. Sougrati, M.-L. Doublet, D. Foix, D. Gonbeau, W. Walker, A. S. Prakash, M. Ben Hassine, L. Dupont, J.-M. Tarascon, *Nat. Mater.* **2013**, *12*, 827.

[72] X. Li, Y. Qiao, S. H. Guo, Z. M. Xu, H. Zhu, X. Y. Zhang, Y. Yuan, P. He, M. Ishida, H. S. Zhou, *Adv. Mater.* **2018**, *30*, 1705197.

[73] A. R. Armstrong, A. D. Robertson, P. G. Bruce, *J. Power Sources* **2005**, *146*, 275.

[74] Y. Okamoto, *J. Electrochem. Soc.* **2012**, *159*, A152.

[75] K. Kubota, T. Kaneko, M. Hirayama, M. Yonemura, Y. Imanari, K. Nakane, R. Kanno, *J. Power Sources* **2012**, *216*, 249.

[76] M. D. Radin, J. Vinckeviciute, R. Seshadri, A. Van der Ven, *Nat. Energy* **2019**, *4*, 639.

[77] S. Y. Shen, Y. H. Hong, F. C. Zhu, Z. M. Cao, Y. Y. Li, F. S. Ke, J. J. Fan, L. L. Zhou, L. N. Wu, P. Dai, M. Z. Cai, L. Huang, Z. Y. Zhou, J. T. Li, Q. H. Wu, S. G. Sun, *ACS Appl. Mater. Interfaces* **2018**, *10*, 12666.

[78] R. Xiao, H. Li, L. Chen, *Chem. Mater.* **2012**, *24*, 4242.

[79] E. McCalla, A. M. Abakumov, M. Saubanere, D. Foix, E. J. Berg, G. Rousse, M.-L. Doublet, D. Gonbeau, P. Novak, G. Van Tendeloo, R. Dominko, J.-M. Tarascon, *Science* **2015**, *350*, 1516.

[80] R. Z. Yu, Z. J. Zhang, S. Jamil, J. C. Chen, X. H. Zhang, X. Y. Wang, Z. H. Yang, H. B. Shu, X. K. Yang, *ACS Appl. Mater. Interfaces* **2018**, *10*, 16561.

[81] a) M. Li, J. Lu, *Science* **2020**, *367*, 979; b) S. W. Zhong, M. Z. Lai, W. L. Yao, Z. C. Li, *Electrochim. Acta* **2016**, *212*, 343; c) T. C. Liu, L. Yu, J. J. Liu, J. Lu, X. X. Bi, A. Dai, M. Li, M. F. Li, Z. X. Hu, L. Ma, D. Luo, J. X. Zheng, T. P. Wu, Y. Ren, J. G. Wen, F. Pan, K. Amine, *Nat. Energy* **2021**, *6*, 277; d) E. Boivin, N. Guerrini, R. A. House, J. G. Lozano, L. Jin, G. J. Rees, J. W. Somerville, C. Kuss, M. R. Roberts, P. G. Bruce, *Adv. Funct. Mater.* **2021**, *31*, 2003660; e) D. Ye, B. Wang, Y. Chen, G. Han, Z. Zhang, D. H. Jurcakova, J. Zou, L. Wang, *J. Mater. Chem. A* **2014**, *2*, 18767.

[82] a) H. Koga, L. Croguennec, M. Ménétrier, P. Mannessiez, F. Weill, C. Delmas, S. Belin, *J. Phys. Chem. C* **2014**, *118*, 5700; b) H. Koga, L. Croguennec, M. Menetrier, K. Douhil, S. Belin, L. Bourgeois, E. Suard, F. Weill, C. Delmas, *J. Electrochem. Soc.* **2013**, *160*, A786.

[83] A. Grimaud, W. T. Hong, Y. Shao-Horn, J. M. Tarascon, *Nat. Mater.* **2016**, *15*, 121.

[84] M. G. Kim, N. E. Sung, H. J. Shin, N. S. Shin, K. S. Ryu, C. H. Yo, *Electrochim. Acta* **2004**, *50*, 501.

[85] X. Y. Zhang, Y. Qiao, S. H. Guo, K. Z. Jiang, S. Xu, H. Xu, P. Wang, P. He, H. S. Zhou, *Adv. Mater.* **2019**, *31*, 1807770.

[86] G. Assat, D. Foix, C. Delacourt, A. Iadecola, R. Dedryvere, J. M. Tarascon, *Nat. Commun.* **2017**, *8*, 2219.

[87] Z. Lu, J. R. Dahn, *J. Electrochem. Soc.* **2002**, *149*, A815.

[88] P. K. Nayak, E. M. Erickson, F. Schipper, T. R. Penki, N. Munichandraiah, P. Adelhelm, H. Sclar, F. Amalraj, B. Markovsky, D. Aurbach, *Adv. Energy Mater.* **2018**, *8*, 1702397.

[89] a) A. R. Armstrong, M. Holzapfel, P. Novák, C. S. Johnson, S.-H. Kang, M. M. Thackeray, P. G. Bruce, *J. Am. Chem. Soc.* **2006**, *128*, 8694; b) Y. Lei, J. Ni, Z. Hu, Z. Wang, F. Gui, B. Li, P. Ming, C. Zhang, Y. Elias, D. Aurbach, Q. Xiao, *Adv. Energy Mater.* **2020**, *10*, 2002506; c) Z. Chen, J. Li, X. C. Zeng, *J. Am. Chem. Soc.* **2019**, *141*, 10751; d) A. Yamano, M. Morishita, M. Yanagida, T. Sakaia, *J. Electrochem. Soc.* **2015**, *162*, A1730.

[90] X. D. Zhang, J. L. Shi, J. Y. Liang, Y. X. Yin, J. N. Zhang, X. Q. Yu, Y. G. Guo, *Adv. Mater.* **2018**, *30*, 1801751.

[91] K. Luo, M. R. Roberts, R. Hao, N. Guerrini, D. M. Pickup, Y. S. Liu, K. Edström, J. H. Guo, A. V. Chadwick, L. C. Duda, P. G. Bruce, *Nat. Chem.* **2016**, *8*, 684.

[92] S. E. Renfrew, B. D. McCloskey, *J. Am. Chem. Soc.* **2017**, *139*, 17853.

[93] M. Oishi, C. Yogi, I. Watanabe, T. Ohta, Y. Orikasa, Y. Uchimoto, Z. Ogumi, *J. Power Sources* **2015**, *276*, 89.

[94] S. Han, Y. Xia, Z. Wei, B. Qiu, L. Pan, Q. Gu, Z. Liu, Z. Guo, *J. Mater. Chem. A* **2015**, *3*, 11930.

[95] D. H. Seo, J. Lee, A. Urban, R. Malik, S. Y. Kang, G. Ceder, *Nat. Chem.* **2016**, *8*, 692.

[96] J. R. Croy, J. S. Park, F. Dogan, C. S. Johnson, B. Key, M. Balasubramanian, *Chem. Mater.* **2014**, *26*, 7091.

[97] F. Dogan, J. R. Croy, M. Balasubramanian, M. D. Slater, H. Iddir, C. S. Johnson, J. T. Vaughey, B. Key, *J. Electrochem. Soc.* **2015**, *162*, A235.

[98] T. Nakamura, H. Z. Gao, K. Ohta, Y. Kimura, Y. Tamenori, K. Nitta, T. Ina, M. Oishi, K. Amezawa, *J. Mater. Chem. A* **2019**, *7*, 5009.

[99] Y. T. Ma, P. F. Liu, Q. S. Xie, G. B. Zhang, H. F. Zheng, Y. X. Cai, Z. Li, L. Wang, Z. Z. Zhu, L. Q. Mai, D. L. Peng, *Nano Energy* **2019**, *59*, 184.

[100] S. Hy, F. Felix, J. Rick, W. N. Su, B. J. Hwang, *J. Am. Chem. Soc.* **2014**, *136*, 999.

[101] A. D. Robertson, P. G. Bruce, *Chem. Commun.* **2002**, *23*, 2790.

[102] A. D. Robertson, P. G. Bruce, *Chem. Mater.* **2003**, *15*, 1984.

[103] S. Venkatraman, A. Manthiram, *J. Solid State Chem.* **2004**, *177*, 4244.

[104] A. R. Armstrong, P. G. Bruce, *Electrochem. Solid-State Lett.* **2004**, *7*, A1.

[105] J. B. Goodenough, Y. Kim, *Chem. Mater.* **2010**, *22*, 587.

[106] N. Zhang, F. Cheng, J. Liu, L. Wang, X. Long, X. Liu, F. Li, J. Chen, *Nat. Commun.* **2017**, *8*, 405.

[107] J. B. Goodenough, *Acc. Chem. Res.* **2013**, *46*, 1053.

[108] F. Lin, I. M. Markus, D. Nordlund, T. C. Weng, M. D. Asta, H. L. Xin, M. M. Doeff, *Nat. Commun.* **2014**, *5*, 3529.

[109] G. Assat, A. Iadecola, D. Foix, R. Dedryvère, J. M. Tarascon, *ACS Energy Lett.* **2018**, *3*, 2721.

[110] J. M. Paulsen, C. L. Thomas, J. R. Dahn, *J. Electrochem. Soc.* **1999**, *146*, 3560.

[111] Y. X. Zuo, B. Li, N. Jiang, W. S. Chu, H. Zhang, R. Q. Zou, D. G. Xia, *Adv. Mater.* **2018**, *30*, 1707255.

[112] D. Eum, B. Kim, S. J. Kim, H. Park, J. P. Wu, S. P. Cho, G. Yoon, M. H. Lee, S. K. Jung, W. L. Yang, W. M. Seong, K. Ku, O. Tamwattana, S. K. Park, I. Hwang, K. Kang, *Nat. Mater.* **2020**, *19*, 419.

[113] C. Y. Cui, X. L. Fan, X. Q. Zhou, J. Chen, Q. C. Wang, L. Ma, C. Y. Yang, E. Y. Hu, X. Q. Yang, C. S. Wang, *J. Am. Chem. Soc.* **2020**, *142*, 8918.

Shao-Lun Cui earned his B.S. degree in Chemistry from Jilin University in 2017. Currently, he is a Ph.D. student majoring in Materials Science at Nankai University in China. His main research interests focus on Li-rich Mn-based cathode materials for high-energy lithium-ion batteries and gel polymer electrolytes.

Ming-Yue Gao received her B.S. in Engineering from Yantai University in 2019. She is currently a Master student majoring in Materials Engineering at Nankai University, China. Her current research focuses on the advanced cathode materials for lithium-ion batteries.

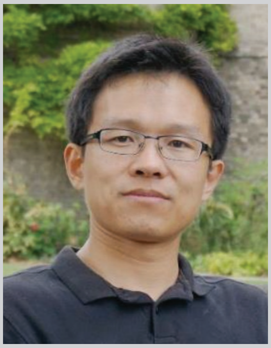

Guo-Ran Li is a professor in Material Chemistry at School of Materials Science and Engineering, Nankai University, China. His main current research interest is the study of new energy materials and devices, and in particular for rechargeable batteries and hybrid solar cells. He received a Bachelor's degree in Chemistry and a Ph.D. degree in Physical Chemistry in 2000 and 2005, respectively, both from Nankai University. He worked as Endeavour Australia Cheung Kong Research Fellow in Queensland University of Technology in 2008 and as a visiting researcher at University of Cambridge from 2014 to 2015.

Xue-Ping Gao is a professor in Institute of New Energy Material Chemistry, Nankai University of China. He received his doctorate at Department of Chemistry from Nankai University in 1995. He worked as a visiting research fellow at Kogakuin University in Japan from 1997 to 1999. Currently, his main research focuses on energy storage materials for power sources, including Li-ion batteries, Li–S batteries, and solar rechargeable batteries.